CM² MAGAZINE

第 45 期

南方科技大学海洋磁学中心主编

创刊词

海洋是生命的摇篮，是文明的纽带。地球上最早的生命诞生于海洋，海洋里的生命最终进化成了人类，人类的文化融合又通过海洋得以实现。人因海而兴。

人类对海洋的探索从未停止。从远古时代美丽的神话传说，到麦哲伦的全球航行，再到现代对大洋的科学钻探计划，海洋逐渐从人类敬畏崇拜幻想的精神寄托演变成可以开发利用与科学研究的客观存在。其中，上个世纪与太空探索同步发展的大洋科学钻探计划将人类对海洋的认知推向了崭新的纬度：深海（deep sea）与深时（deep time）。大洋钻探计划让人类知道，奔流不息的大海之下，埋藏的却是亿万年的地球历史。它们记录了地球板块的运动，从而使板块构造学说得到证实；它们记录了地球环境的演变，从而让古海洋学方兴未艾。

在探索海洋的悠久历史中，从大航海时代的导航，到大洋钻探计划中不可或缺的磁性地层学，磁学发挥了不可替代的作用。这不是偶然，因为从微观到宏观，磁性是最基本的物理属性之一，可以说，万物皆有磁性。基于课题组的学科背景和对海洋的理解，我们对海洋的探索以磁学为主要手段，海洋磁学中心因此而生。

海洋磁学中心，简称 CM^2，一为其全名“Centre for Marine Magnetism”的缩写，另者恰与爱因斯坦著名的质能方程 $E = MC^2$ 对称，借以表达我们对科学巨匠的敬仰和对科学的不懈追求。

然而科学从来不是单打独斗的产物。我们以磁学为研究海洋的主攻利器，但绝不仅限于磁学。凡与磁学相关的领域均是我们关注的重点。为了跟踪反映国内外地球科学特别是与磁学有关的地球科学领域的最新研究进展，海洋磁学中心特地主办 CM^2 Magazine，以期与各位地球科学工作者相互交流学习、合作共进！

“海洋孕育了生命，联通了世界，促进了发展”。 21 世纪是海洋科学的时代，由陆向海，让我们携手迈进中国海洋科学的黄金时代

目 录

研究进展

EPS: 低干扰磁场热退磁炉研发

热退磁炉是古地磁学研究的最常规设备之一。理想的热退磁要求样品保持在零磁场中进行加热冷却处理。实际中总是存在干扰磁场，主要包括退磁炉材料的剩磁造成的静残余磁场和加热电流产生的电流磁场。这些干扰磁场总是会或多或少的影响样品的退磁效果，因此尽量低的干扰磁场是高性能热退磁炉的核心要素。炉腔内静磁的主要由屏蔽筒的剩磁产生，可以对屏蔽筒进行交变退磁优化处理。电流磁场来源于炉丝电流，一般采用无感绕制方式（常规的有双线并行绕制和螺线管对称布置的方式），相邻炉丝互相抵消电流磁场的办法进行处理（图 1）。

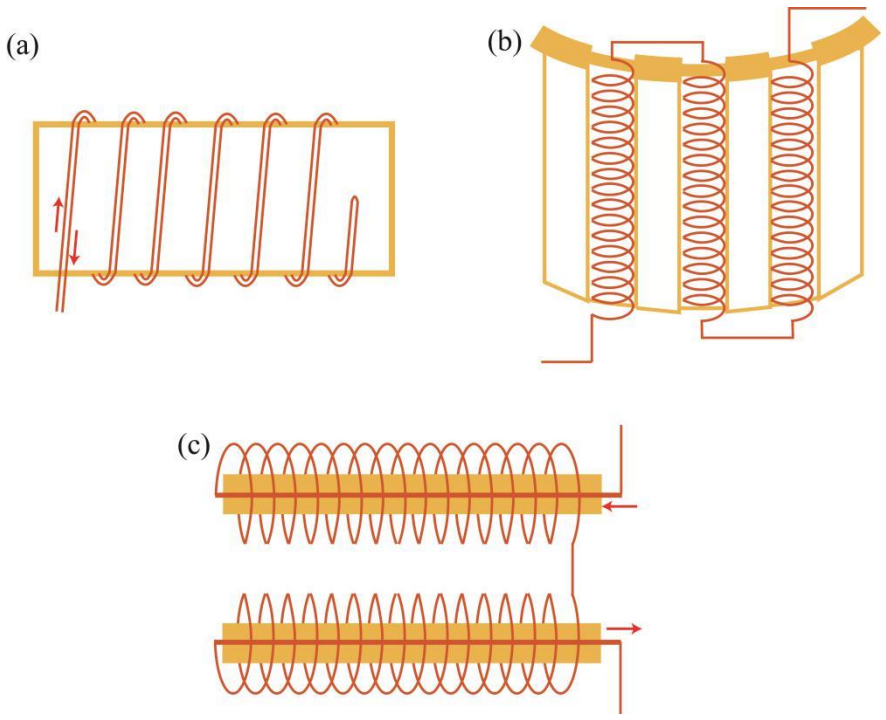

图 1.无感炉丝绕制方式（a)双线并行绕制（b)常规螺线管布置（c）新炉丝结构

通常认为长螺线管的磁场集中在内部，外部的磁场可以忽略。相邻螺线管电流方向可以抵消电流磁场。而模拟和实验均证明的长螺线管外的磁场类似于螺线管中心轴直导线产生的磁场，相邻或者圆对称分布的炉丝并不能完全抵消电流

磁场，导致退磁炉中电流磁场并不均匀，炉腔中心可以很低，越靠近炉丝边缘磁场越高（图 2)。采用中心通入反向电流的直炉丝的螺线管可以明显降低电流磁场。采用这种中心返回直丝的螺线管结构，能够制作性能优异的热退磁炉。

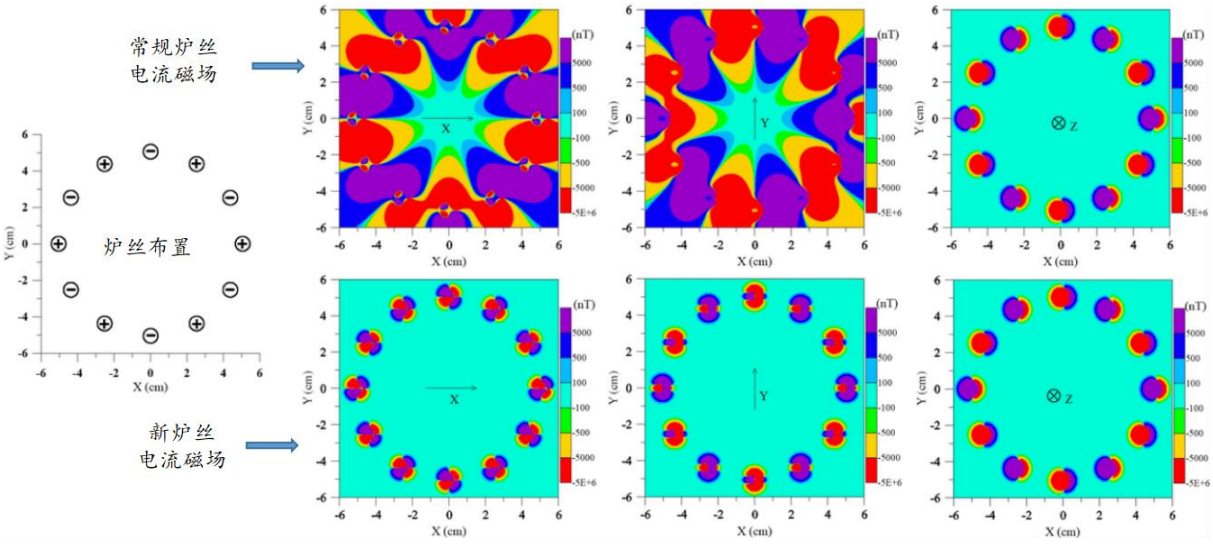

图 2.炉腔中心截面电流磁场分布等值线图

中国科学院地质与地球物理研究所古地磁与年代学实验室团队经过多年努力，尝试不同方法，不断试验，最终采用新的炉丝制作技术研制了新的热退磁炉。磁场测试和样品的热退磁实验均表明该热退磁炉具有十分优异的热退磁效果，与美国 ASC-TD48 热退磁实验结果对比显示新的热退磁炉具有更优的效果（图 3）。该热退磁炉已经在实验室连续运行 3 年，获得了一些很好的数据结果，支持的成果发表在 EPSL、JGR、NSR 等期刊上。该退磁炉对处理弱磁样品，特别是倒转期间或者地球早期的样品以及行星弱磁场环境的样品将会有很大优势。

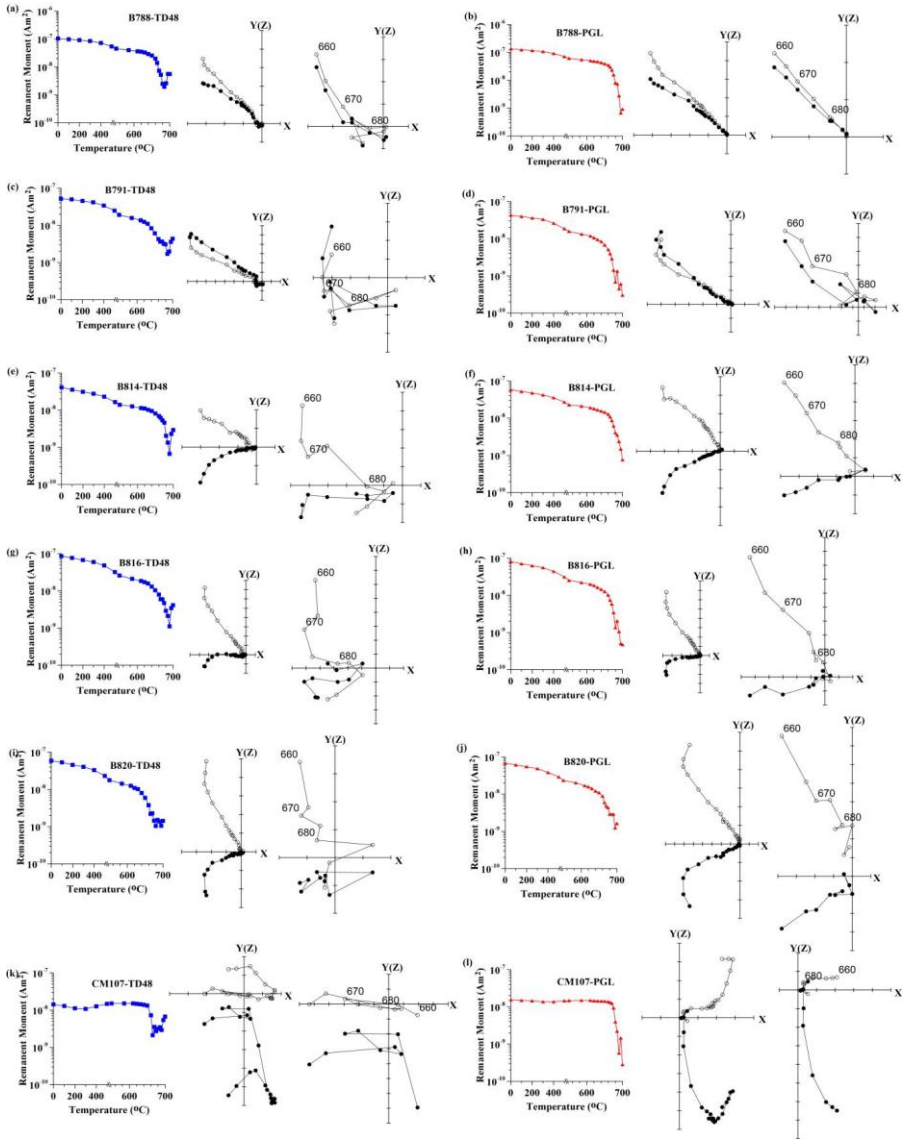

图 3.天然样品热退磁结果（左边蓝色为 TD-48 炉热退磁结果，右边红色为新热退磁炉退磁结果）

该研究成果近期发表于 Earth, Planets and Space（Qin HF, Zhao X, Liu S C, Paterson G A, Jiang Z X, Cai S H, Li J H, Liu Q S, Zhu R X. An ultra-low magnetic field thermal demagnetizer for high-precision paleomagnetism. Earth, Planets and Space, 2020, 72:170.）

作者简介：秦华峰，中国科学院地质与地球物理研所。主要从事古地磁实验方法技术和设备研制。

GRL：磁组构解译地震断层构造滑动机理

近日，南方科技大学海洋科学与工程系（简称“海洋系”）助理教授周祐民在地震断层构造滑动机理研究取得重要研究进展，提供了一种崭新的方法来研究造成地震灾害的活动断层的地震特性。研究成果以“The Magnetic Fabric of Gouge Mimics the Co-seismic Focal Mechanism of the Chi-Chi Earthquake (1999, Mw 7.6)”为题在地球物理学科的自然指数顶级期刊《地球物理研究快报》(Geophysical Research Letters)发表。

地震灾害往往会造成严重的生命财产损失，了解断层的活动机制与评估地震灾害危险是当前地学研究的前沿探索与热点问题。

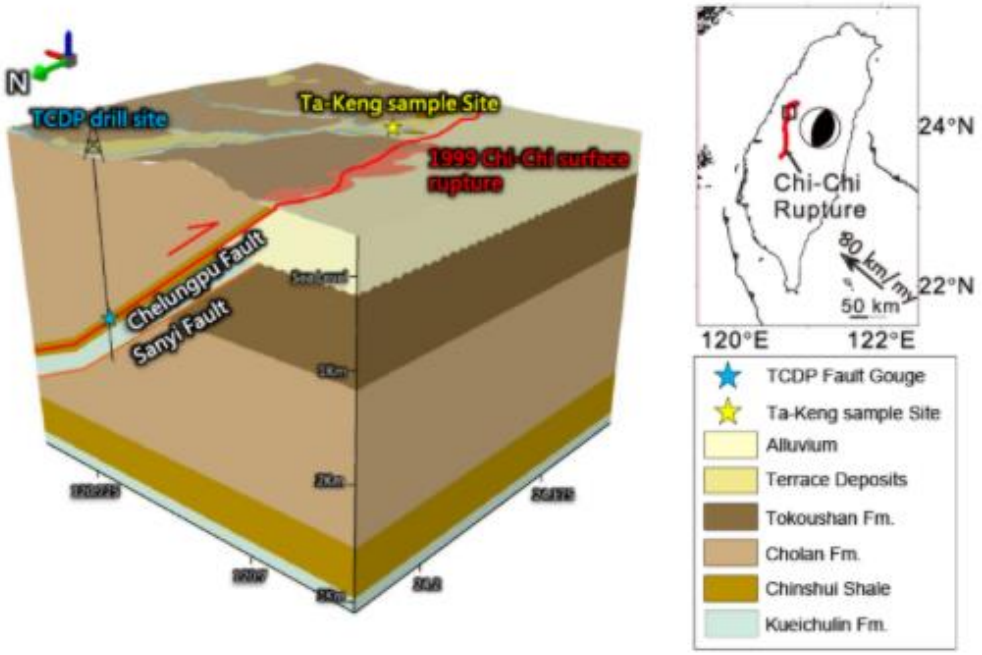

图 1 本研究车笼埔断层 1999 年集集地震断层泥样品位置示意图

什么是断层？如果我们用力折一把直尺，直尺就会断裂，并形成断裂面。岩石地层在受到应力作用时，也会像直尺那样产生断裂，地层沿断裂面两侧发生相对位移，这种地质构造就称之为断裂。人们可以通过地震发生后，地层断裂面的性质，进而了解断层的破裂过程和影响因素。对于近年刚发生的断裂，科学家研究断裂面相对容易。但是，对于古老地震断层，研究难度就大增。

不过，当断层发生破裂错动和位移时，断层面的岩石受到极大的应力挤压与摩擦，在断层面形成微米甚至纳米大小的断层泥。这些断层泥携带着断层活动的多种信息。通过分析断层泥的性质，可获取断层过去的一系列运动学参数，进而了解地震断层的破裂机制。

然而，应用传统方法，科学家分析微米或纳米级断层泥中碎屑颗粒的排列与所受应力的关系，往往费时且费力。如何快速有效地获取上述信息，是一个前沿研究热点问题。周祐民团队另辟新径，针对断层泥的磁学性质进行深入研究。

该磁学方法名为磁化率各项异性法。样品中含有磁性矿物，因而能够被磁化，所以具有磁化率。团队沿着样品的不同方向测量，其磁化率值并不一样，即磁化率各向异性。1999 年，台湾南投县集集镇发生 7.6 级地震。研究团队首次利用该地震在地表与地底一公里处的断层泥样品，通过高精度旋转磁化率仪，测量其磁化率各向异性。研究结果发现，在地震发生断层滑动过程，断层泥中矿物颗粒受到应力作用挤压重新排列，于是产生了特定的磁化率各向异性特征。研究团队通过这种研究方法，确定了磁性矿物颗粒的排列方式。这种研究方法快速高效，同时还不破坏样品。最后，通过磁化率各项异性的系统研究，研究团队有效地分析了地震发生时断层的滑移机制，并进一步判断了断层上下盘的相对运动方向。这些研究结果得到了地震台站资料的验证，说明方法切实有效，这为未来地震活动断层的研究提供了一种新的方法与研究领域。

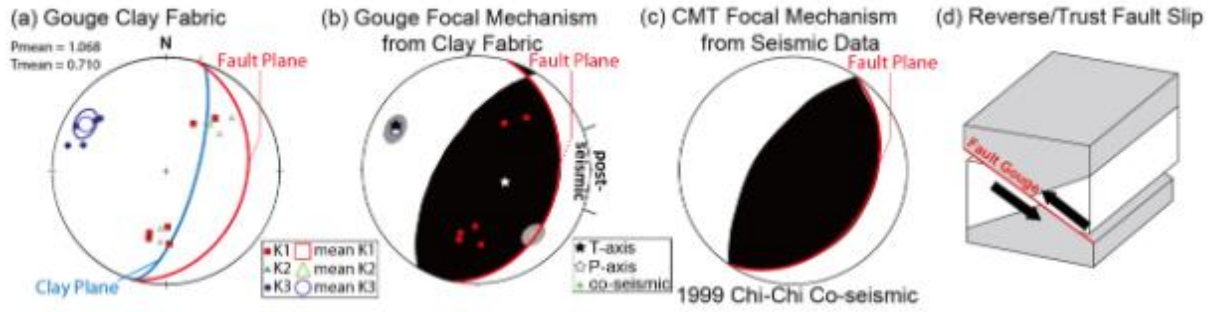

图 2 (a)断层泥的磁组构下半球投影图，K1-最大轴，K2-中间轴，K3-最小轴，黑色线为段层面方位。(b)由断层磁组构回推的地震震源机制解。(c)由地震波资料建立的震源机制解。(d)1999 年集集地震为一逆冲断层破裂所造成。

通过以上分析可知，该研究成果对于深入研究地震断层物理机制具有重要的科学意义，为今后地震灾害预防提供一种新的研究方法。

周祐民为论文第一作者与通讯作者，法国波城大学教授 Charles Aubourg 与台湾师范大学副教授叶恩肇为共同通讯作者，南科大为论文的唯一通讯单位。以上研究得到了深圳市科创委与南科大启动经费的支持。

论文链接： https://doi.org/10.1029/2020GL090111

作者简介： 周祐民，台湾大学和法国赛吉冯图瓦兹大学博士，南方科技大学海洋系助理教授。主要从事海洋地质与环境变迁、活动断层构造、地震断层活动的物理化学机制及古地磁场的长期变化等。

JGR: 天山 K-Pg 时期玄武岩古地磁结果指示磁异常及磁场倒转频率与长期变呈正相关

地磁场是地球最古老的特征之一。《科学》杂志列出的 125 个需要回答的科学问题，以及美国国家研究理事会发布的《时域地球——美国国家科学基金会地球科学十年愿景（2020-2030）》第 1 个科学优先问题，将“地磁场如何产生和如何倒转”列入其中。古地磁研究表明，地磁场倒转频率可能受到核幔边界热状态的影响，呈现地磁极性频繁倒转与数百万年保持不变的超静磁期的特征。160 Ma 以来地磁极性年代可以分为四个阶段，分别为 0-40Ma 每百万年倒转 4 次，40-80Ma 每百万年倒转 1.3 次，83-123Ma 超静磁期，120-160Ma 每百万年倒转 2.4 次。那么，关键科学问题是获得磁极性倒转频率与哪些地磁场特征有关。具体来讲，磁极性倒转频率是否与表征地磁场长期变化的磁场强度以及虚地磁极离散度相关？在精确的时代框架下准确的定量估算地磁场长期变化是解决这一科学问题的基本前提。然而，一方面离散度受纬度影响，并被质疑无法表征地磁发电机的特征。另一方面，与纬度无关的古强度变化却存在较低的实验成功率。与此同时，白垩纪-新生代期间中亚地区磁倾角异常低于预期值一直是困扰学术界的科学难题，并影响到了我们正确理解印度-欧亚碰撞的构造重建。

针对以上科学问题，中国地质大学（北京）地球科学与资源学院王成善院士团队孟俊副教授与德国慕尼黑大学 Florian Lhuillier 博士合作，对中亚西天山托云地区 K-Pg 时期玄武岩（图 1）开展了详细的古地磁学研究，获得如下实验结果：93 个组（129 个熔岩流采点）方向数据得出西天山托云地区 60-70Ma 虚地磁极为 180.2°E，49.5°N，离散度 S = 20.8° (18.8°, 23.1°)。磁倾角 I = 36.2°表明托云火山岩喷发于~20°N，远远低于同时期欧亚/东亚板块预期的磁倾角（图 2）。绝对古强度实验获得地磁场虚偶极矩 58.9 ± 6.9 ZA·m2，与全球数据库 60-70Ma 古强度吻合（图 3）。Pseudo-Thellier 实验获得相对强度变化 31 ± 5% (N= 15)，与地磁场倒转频率呈正相关（图 3）。以上结果表明：

（1）对比红层古地磁结果，天山地区 K-Pg 时期火山岩同样存在磁倾角异常低的特征。印度-欧亚大陆碰撞导致的地壳缩短不能完全解释 10-15°的磁倾角异常，因此，地磁场局部异常也是导致中亚地区低磁倾角的机制之一。

（2）古强度实验结果可能支持 120Ma 以来地磁场倒转频率与长期变的正相关性。

上述研究成果发表在地球科学国际权威刊物《Journal of Geophysical Research: Solid Earth》上：Meng, J., Lhuillier, F., Wang, C., Liu, H., Eid, B., & Li, Y. 2020. Paleomagnetism of Paleocene-Maastrichtian (60-70 Ma) lava flows from Tian Shan (Central Asia): Directional analysis and paleointensities. Journal of Geophysical Research: Solid Earth, 125(9), e2019JB018631. https://doi.org/10.1029/2019JB018631 [IF=3.64].

作者简介： 孟俊，博士，副教授，博士生导师，主要从事古地磁学、构造地质学等方向的教学科研工作。曾获朱训青年教师奖，全国高校微课教学比赛北京市三等奖，国土资源科学技术二等奖。

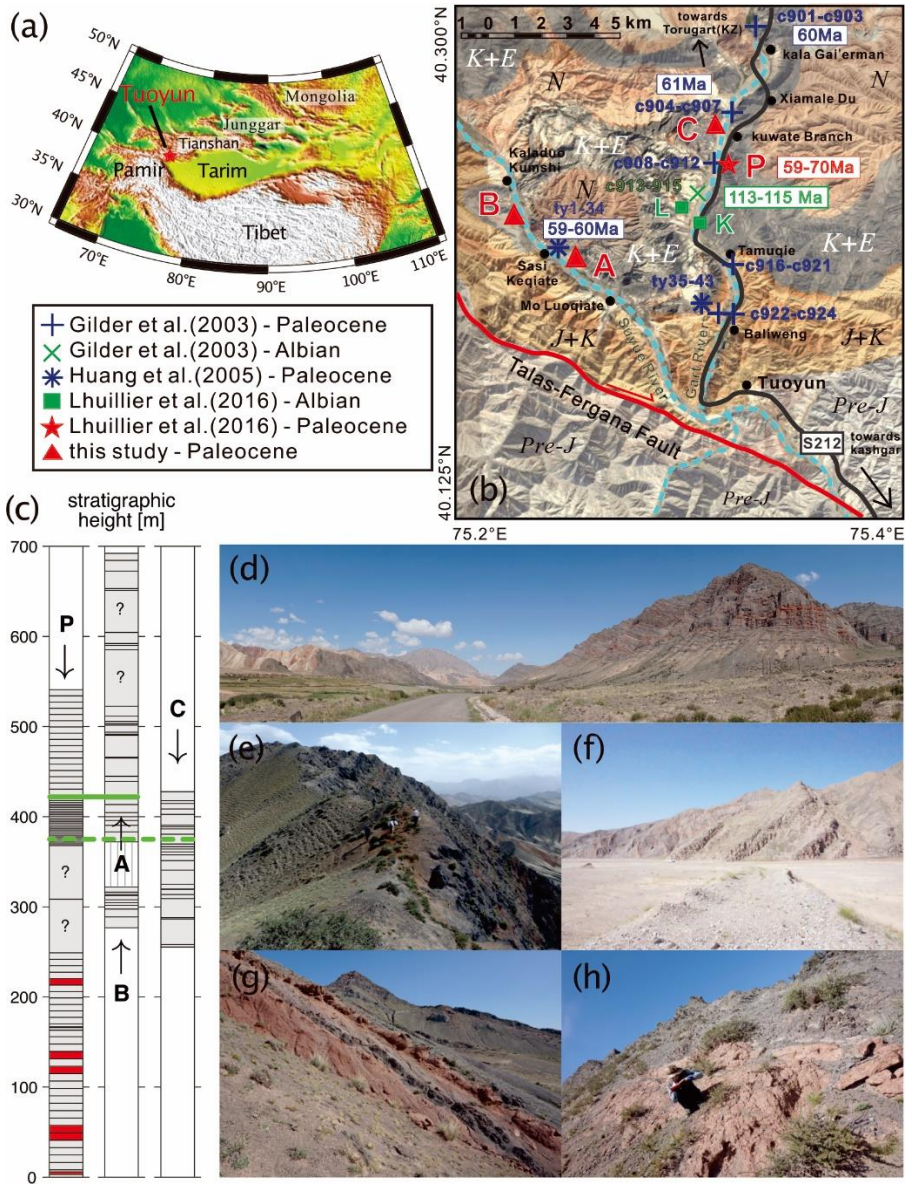

图 1 中亚西天山托云地区地质背景与 K-Pg 玄武岩剖面信息

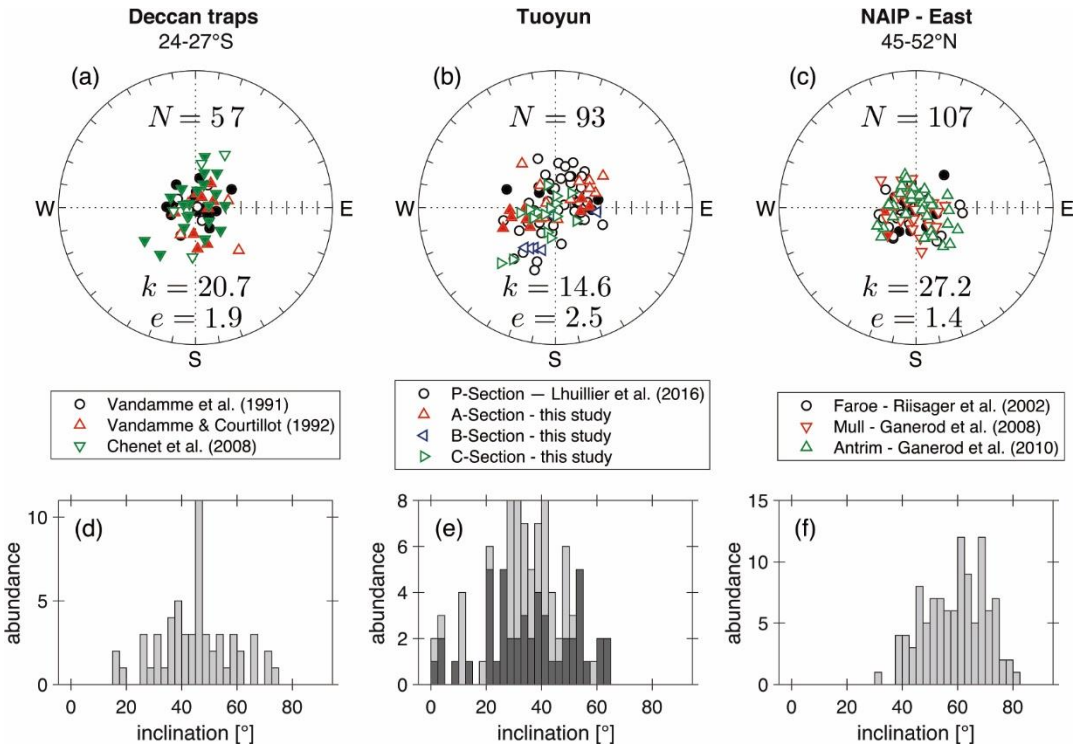

图 2　同时期（~60Ma）德干玄武岩、托云玄武岩与北大西洋大火成岩省的古地磁方向数据对比

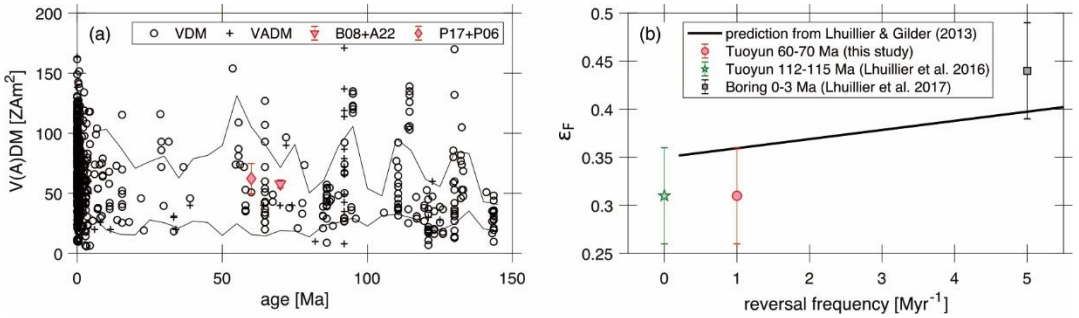

图 3 托云地区 K-Pg 玄武岩绝对/相对古强度实验结果与全球古强度数据对比

JGR：中-晚二叠世东亚构造古地理演化与生物多样性变化的关系

构造古地理演化与古生物多样性变化事件存在的因果关系一直是研究地球演化历史中引人注目的科学问题。在二叠纪时期，东亚地区几乎同时发生了两方面重要的地质事件，一方面是古亚洲洋的闭合形成了索伦缝合线，其演化决定了东亚大地构造基本格架的形成；另一方面是古赤道生物区和北方生物区的生物多样性变化，主要包括瓜德鲁普晚期海洋底栖动物大灭绝以及华夏植物群和安加拉植物群的混生事件。许多研究表明索伦缝合线是一条重要的生物古地理分界线，发现北侧的腕足动物群多样性在瓜德鲁普晚期突然明显减少（如哲斯动物群），以及华夏-安加拉植物群混生年代沿缝合线自西向东逐渐变年轻。但是，由于古亚洲洋闭合时间与方式还存在很大的争议，所以这些生物事件与洋盆关闭在时空上的因果关系仍不明确。

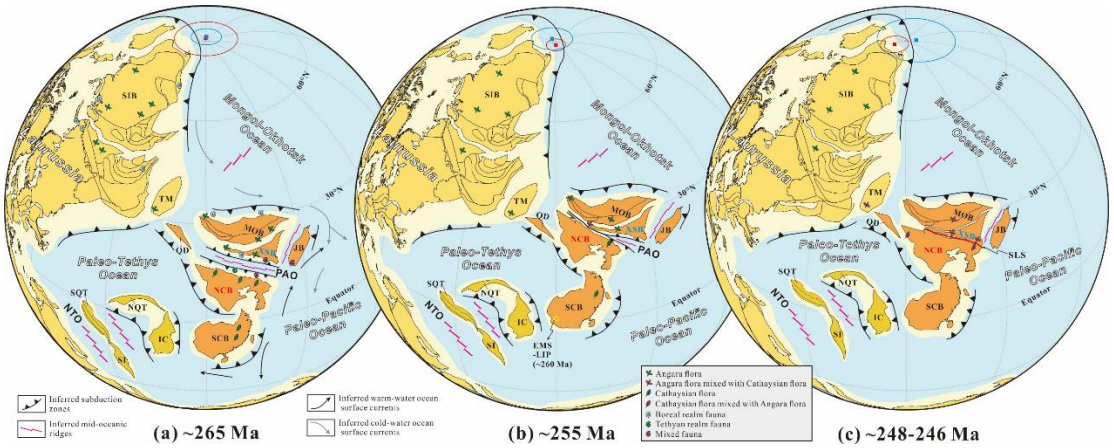

图 1　~265-246 Ma 古地理重建图

针对上述重要科学问题，中国地质大学（北京）博士后任强在张世红教授的指导下，在索伦缝合线两侧锡林浩特地块和华北地块的中二叠统哲斯组红层和上二叠统青凤山组上部火山岩和砂岩分别开展详细的年代学和古地磁学研究，取得以下重要成果：

（1）获得锡林浩特地块哲斯组（~265 Ma）红层和华北地块青凤山组上部（~255 Ma）的高质量古地磁极；

（2）通过对比锡林浩特地块和华北地块二叠纪高质量古地磁极，揭示两地块在 265-246 Ma 之间存在一定程度的纬向汇聚和相对旋转运动，此运动方式

导致古亚洲洋（索伦洋）自西向东“剪刀式”闭合，并在时空上控制了华夏-安加拉植物群的混生过程；

（3）在 265-255 Ma 期间，锡林浩特地块、华北地块甚至东亚其它地块都同时经历了快速的向北运动，这样快速的板块运动可能成为东亚地区海洋生物在瓜德鲁普晚期的大灭绝重要因素之一。

上述研究成果发表在地球科学国际权威刊物《Journal of Geophysical Research: Solid Earth》上：Ren, Q., Zhang, S., Gao, Y., Zhao, H., Wu, H., Yang, T., & Li, H. (2020). New Middle‐Late Permian paleomagnetic and geochronological results from Inner Mongolia and their paleogeographic implications. Journal of Geophysical Research: Solid Earth, 125, e2019JB019114. https://doi.org/10.1029/2019JB019114.

作者简介：任强，现工作于成都理工大学沉积地质研究院，从事构造古地磁学和磁性地层学研究。本科毕业于成都理工大学，在中国地质大学（北京）获得构造地质学博士学位。2018-2020 年在中国地质大学（北京）海洋学院从事博士后研究工作。2020 年 9 月被成都理工大学“珠峰人才计划”引进。

第 35 章　磁性参数综合定性解释

单一磁性参数解释起来存在多解性，大部分情况下，我们需要组合多参数特征，提高信息量，减少多解性。我们选取最为常见的四个参数为例子，探讨他们之间的相互制约关系。这四个参数是χ、χ_{fd}、ARM、SIRM。每一种参数都对应着三种状态，增加（↑）、不变（□）、减小（↓）。我们来讨论其中一些代表性的模式：

1）χ（↑）、χ_{fd}（↑）、ARM（↑）、SIRM（↑）

2）χ（↓）、χ_{fd}（↓）、ARM（↓）、SIRM（↓）

这两种情况相对来说比较好解释，所有参数同甘共苦，共进退。如果 ARM/SIRM 变化不大，这基本上表示粒径影响不大，磁性矿物含量变化导致所有磁性参数的变化。

我们把问题稍微复杂一点点，在其它参数升高的时候，SIRM 不增加，反而下降：

3）χ（↑）、χ_{fd}（↑）、ARM（↑）、SIRM（↓）

可不要小看这一点变化，解释起来就复杂多了。首先，这告诉我们含量变化就不是唯一因素了，粒径变化的影响不容忽视。ARM/SIRM 比值变高，说明颗粒粒径变小。χ（↑）、χ_{fd}（↑）、ARM（↑）三者增加，说明 SP+SD 的含量增加，而大颗粒成分减少很多。

4）χ（↓）、χ_{fd}（↓）、ARM（↓）、SIRM（↑）

第四种情况和第三种刚好反过来，这可不是同样一种情况。ARM/SIRM 减小，这说明粒径整体变粗，SP+SD 的含量降低。

现在我们把第三种情况改变一下，把 ARM 和 SIRM 的状态互换：

5）χ（↑）、χ_{fd}（↑）、ARM（↓）、SIRM（↑）

此时，ARM 随着其它参数的增加反而降低，这又是什么情形呢？

显然χ（↑）和χ_{fd}（↑）以及 SIRM（↑）正相关，说明样品的磁化率主要受到 SP 颗粒的影响，PSD/MD 颗粒的贡献也很明显。SD 颗粒对磁化率贡献不

大，所以 ARM 降低对磁化率本身影响不大。对比 ARM 和 SIRM，ARM/SIRM 比值降低，说明颗粒粒径整体变粗，所以虽然 ARM 降低，但是粗颗粒对 SIRM 的贡献超过 SD 颗粒，乃至于其整体 SIRM 还是增加。这个过程看起来有点怪异，除了 SD 颗粒含量降低，SP 和 MD 颗粒的含量都增加了。

如果我们把 5）中的χ_{fd}和 ARM 对调一下，会是什么情况：

6）χ（↑）、χ_{fd}（↓）、ARM（↑）、SIRM（↑）

这种情况下，ARM/SIRM 很快可能变化不大，也就是说能够携带剩磁的部分颗粒整体含量增加了。因为 MD 颗粒也具有较大的磁化率，所以样品磁化率增加一点也不奇怪。χ_{fd}降低，说明 SP 颗粒含量减少，但是 SP 颗粒减少对样品的磁化率没有造成很大影响，这说明 SP 颗粒含量很小，或者 MD 含量的增加补偿了 SP 含量的降低，整体磁化率反而上升。

这就引出了第七种情况：

7）χ（↓）、χ_{fd}（↓）、ARM（↑）、SIRM（↑）

在第七种情况里，磁化率参数都降低，而剩磁都升高。这说明样品的磁化率主要受到 SP 颗粒控制，SP 含量降低当然对剩磁没影响。正常情况下，SP 和 SD 颗粒会同时存在，即使 SD 颗粒含量也随之减少，但是 MD 颗粒大幅度增加也会引起 ARM 的增加，但是没有能补偿 SP 颗粒含量降低造成的磁化率较少。

我们把第七种情况两两对调：

8）χ（↑）、χ_{fd}（↑）、ARM（↓）、SIRM（↓）

磁化率参数都增加，而剩磁参数都降低。很明显，剩磁携带者对样品的磁化率贡献不大，估计含量较低。样品磁化率的变化主要受到 SP 颗粒的控制。

现在我们让参数的变化交错一下：

9）χ（↑）、χ_{fd}（↓）、ARM（↑）、SIRM（↓）

频率磁化率和 SIRM 降低，而磁化率和 ARM 增加。看起来 SP 颗粒对样品整体磁化率影响不大，SP 含量不高。ARM 大幅度增加，且 ARM/SIRM 增加，这说明颗粒粒径整体向细颗粒移动（MD→PSD→SD），同时细颗粒的含量大幅度增加。

下面，我们再考察某些参数不变的情况。还是从第一种情况开始，让 SIRM 保持不变：

10）χ（↑）、χ_{fd}（↑）、ARM（↑）、SIRM（□）

这说明 SP+SD 颗粒含量增加，是造成磁化率增加的主要机制。ARM 增加，肯定会引起 SIRM 增加，但是实际情况 SIRM 并没有变化，这就需要 PSD/MD 颗粒含量降低加以补偿，磁性颗粒的粒径必然会向细颗粒移动，这和 ARM/SIRM 增加时一致的。

11）χ（↑）、χ_{fd}（↑）、ARM（□）、SIRM（↑）

现在我们来到第 11 种情况，其他参数增加，而 ARM 保持不变。磁化率和频率磁化率同时增加，这很好理解，可以认为磁化率受到 SP 颗粒的控制，SIRM 增加，而 ARM 不增加，说明 SD 颗粒对 SIRM 贡献很小，所以 SIRM 增加主要是大颗粒 MD 含量增加引起的。ARM 保持不变，这就需要 SD 的含量降低，从而整体粒径向大颗粒方向移动，这和 ARM/SIRM 降低是一致的。

我们把中间两个参数互换一下：

12）χ（↑）、χ_{fd}（□）、ARM（↑）、SIRM（↑）

此时，除了频率磁化率，其他参数都增加。这说明样品的磁化率不受到 SP 颗粒控制，而主要受到大颗粒含量增加控制。因此，样品整体粗颗粒增加，而 SP 颗粒保持不变。ARM 的增加看起来主要也是由于粗颗粒整体含量增加引起的，而并非是真正的 SD 含量增加了？？。

我们把χ和χ_{fd}的状态互换一下：

13）χ（□）、χ_{fd}（↑）、ARM（↑）、SIRM（↑）

χ是一个综合参数，所有成分对它有贡献。其它参数都增加，而磁化率居然不变，这看起来匪夷所思。我们来思考一下，SP 和大颗粒 MD 对磁化率都贡献很大。χ_{fd} 增加，毋庸置疑，SP 含量增加了，这应该造成磁化率增加。ARM 和 SIRM 增加，这表明至少 SD 含量增加了。如果 MD 含量也增加，整体磁化率必然会增加，这与观测结果相矛盾。所以，对于 13）这种情况，只能是 MD 颗粒含量降低，抵消了 SP 颗粒含量增加，从而使得整体磁化率持平。SD 含量加，ARM 和 SIRM 都会增加，但是 SD 颗粒对磁化率贡献很小。总结一下就是，SP+SD 含量增加，MD 含量减少。我们还可以预测，虽然 ARM 和 SIRM 都增加，但是 ARM/SIRM 必然要增加。

这种参数变化情形非常多，若干在加入另外一种参数，我们就没办法一一枚举了。只有掌握好各个参数的物理机制及复杂影响因素，我们及可以以逸待劳，以不变应万变。如果只死记硬背，面对新情况时，还会茫然失措。

文献速递

1. 中亚地区新生代以来草原-荒漠化生态圈的演化历史

翻译人：仲义 zhongy@sustech.edu.cn

N. Barbolini, A. Woutersen*, G. Dupont-Nivet et al.,* ***Cenozoic evolution of the steppe-desert biome in Central Asia*** *[J]* ***Science Advance****, 2020, 6(41), eabb8227.*

https://advances.sciencemag.org/content/6/41/eabb8227

摘要：中亚地区的干旱和季节性的阶梯式草原-荒漠化生物群落的起源和发展是世界上最大的生物群落，但是至今还没有很好的记录。我们尚不清楚新生代的气候、地质和生物应力是如何在不同空间和时间尺度上塑造中亚的生态系统。综合分析表明，中亚地区草原-荒漠至少从始新世以来就已经存在，且至少经历两次转变，一次发生在始新世-渐新世，一次发生在中新世中期。这些转换进而分离出三个连续的“稳定状态”，每一个都具有独特的植物和动物结构特征。根据过去对亚洲草原-荒漠干预的响应表明，如果草原-荒漠被迫进入一个新的机制中，现代生态系统就无法再恢复目前的结构和多样性。这是今天亚洲大草原所关切的重要问题，因为他们正在被改造以供人类使用，并以前所未有的速度消失于荒漠之中。

ABSTRACT: The origins and development of the arid and highly seasonal steppe-desert biome in Central Asia, the largest of its kind in the world, remain largely unconstrained by existing records. It is unclear how Cenozoic climatic, geological, and biological forces, acting at diverse spatial and temporal scales, shaped Central Asian ecosystems through time. Our synthesis shows that the Central Asian steppe-desert has existed since at least Eocene times but experienced no less than two regime shifts, one at the Eocene-Oligocene Transition and one in the mid-Miocene. These shifts separated three successive “stable states,” each characterized by unique floral and faunal structures. Past responses to disturbance in the Asian steppe-desert imply that modern ecosystems are unlikely to recover their present structures and diversity if forced into a new regime. This is of concern for Asian steppes today, which are being modified for human use and lost to desertification at unprecedented rates.

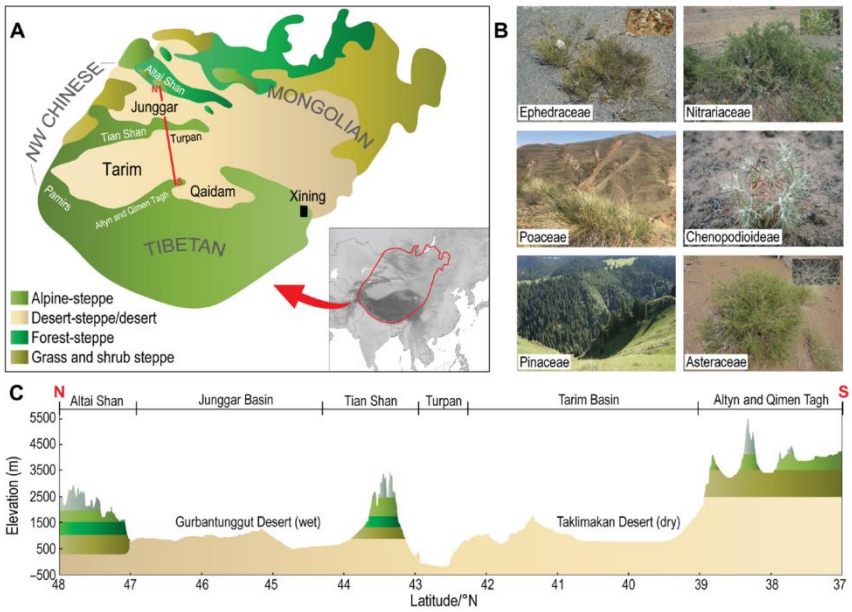

Figure 1. The modern Central Asian steppe-desert. (A) Ecological-physiognomic steppe subtypes across the Tibetan, northwestern (NW) Chinese, and Mongolian regions, with sedimentary basins and mountain ranges marked in black and white, respectively [after (1, 11, 97)]. Location of the altitudinal profile in (C) is marked in red. (B) Characteristic plant families, represented by (clockwise from top left): Ephedra sp. (Ephedraceae), Nitraria sp. (Nitrariaceae), Ceratocarpus sp. (Chenopodioideae), and Artemisia sp. (Asteraceae): all common in desert steppe and desert; Picea sp. (Pinaceae: common in forest steppe); and Achnatherum sp. (Poaceae: common in grass and shrub steppe). The latter image was photographed in the Xining Basin, Qinghai Province (photo credit: Natasha Barbolini, University of Amsterdam); all other images were taken on the southern margin of the Junggar Basin/northern slope of the Tian Shan, Xinjiang Uyghur Autonomous Region (photo credits: Hong-Xiang Zhang, Xinjiang Institute of Ecology and Geography, Chinese Academy of Sciences). (C) Altitudinal profile illustrating vegetation belts of steppe subtypes shown in (A), with tundra and periglacial in gray.

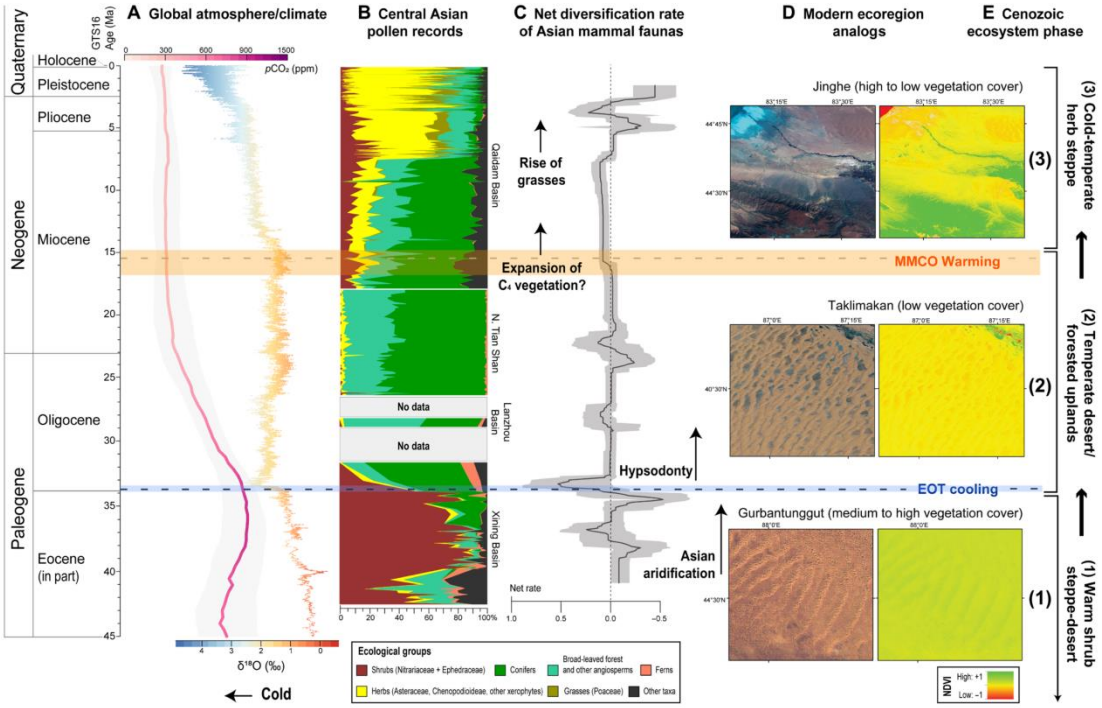

Figure 2. The triphase Cenozoic history of the Central Asian steppe-desert biome. Vegetation changes are illustrated by a composite pollen record over the last ~43 Ma (B), within the context of global climate variation (A) and linked to net diversification rates of Central Asian mammalian communities (C). Extant Asian deserts are used as ecoregion analogs (D) for each ecosystem phase (E) and illustrated by natural view [left; images from Landsat 8 OLI (Operational Land Imager), https://glovis.usgs.gov/] and hyperspectral (right) normalized difference vegetation index (NDVI) models of the (1) Gurbantunggut Desert, (2) Taklimakan Desert, and (3) Jinghe mountain–desert ecotone. Atmospheric carbon dioxide concentration (pCO_2) is based on a LOESS (locally estimated scatterplot smoothing) fit through data from various proxy methods (163), enveloped by a 95% confidence interval in light gray. Global climate is represented by a nine-point moving average through the benthic foraminifera $\delta^{18}O$ record of Cramer et al. (166). For individual pollen records, see fig. S1; for statistical support of the three ecosystem phases, see fig. S3.

2. 伟晶岩中晶体快速生长的片段

翻译人：冯婉仪 fengwy@sustech.edu.cn

Phelps P R, Lee C T A, Morton D M. ***Episodes of fast crystal growth in pegmatites****[J].* ***Nature communications****, 2020, 11: 4986. https://doi.org/10.1038/s41467-020-18806-w*

摘要：伟晶岩是一种浅层的、粗粒的岩浆侵入体，其晶体粒径有时可达数米长。与它们的深成宿主岩体相比，伟晶岩被认为冷却得很快，这表明这些大晶体生长得很快。然而，它们的生长速度和条件仍没有被很好地约束。在这里，我们研究了来自美国南加州斯图尔特伟晶岩晶洞中的石英晶体及其微量元素组成来量化其晶体生长速率。石英晶体中的微量元素浓度明显偏离平衡状态，用与晶体快速生长相关的动力学效应能很好的解释这一现象。晶体生长动力学理论被用来显示晶体从最初的 10^{-6}-10^{-7} m s $^{-1}$ 加速到 10^{-5}-10^{-4} m s $^{-1}$（每日生长 10-100 mm 到每日生长 1-10 m），这表明如果在伟晶岩形成过程中晶体生长保持这种速率，那么在几天内就可以形成数米大小的晶体。高的生长速率要求石英晶体从流体-晶体界面的薄（微米级）化学边界层生长。这样薄的边界层需要一个强大的平流分量来维持。在结晶过程中，这些晶洞中存在动荡的条件（高雷诺数），表明挥发份出溶、结晶和晶洞形成同时发生。

ABSTRACT: Pegmatites are shallow, coarse-grained magmatic intrusions with crystals occasionally approaching meters in length. Compared to their plutonic hosts, pegmatites are thought to have cooled rapidly, suggesting that these large crystals must have grown fast. Growth rates and conditions, however, remain poorly constrained. Here we investigate quartz crystals and their trace element compositions from miarolitic cavities in the Stewart pegmatite in southern California, USA, to quantify crystal growth rates. Trace element concentrations deviate considerably from equilibrium and are best explained by kinetic effects associated with rapid crystal growth. Kinetic crystal growth theory is used to show that crystals accelerated from an initial growth rate of 10^{-6}-10^{-7} m s^{-1} to 10^{-5}-10^{-4} m s^{-1} (10-100 mm day^{-1} to 1-10 m day^{-1}), indicating meter sized crystals could have formed within days, if these rates are sustained throughout pegmatite formation. The rapid growth rates require that quartz crystals grew from thin (micron scale) chemical boundary layers at the fluid-crystal interfaces. A strong advective component is required to sustain such thin boundary layers. Turbulent conditions (high Reynolds number) in these miarolitic cavities are shown to exist during crystallization, suggesting that volatile exsolution,

crystallization, and cavity generation occur together.

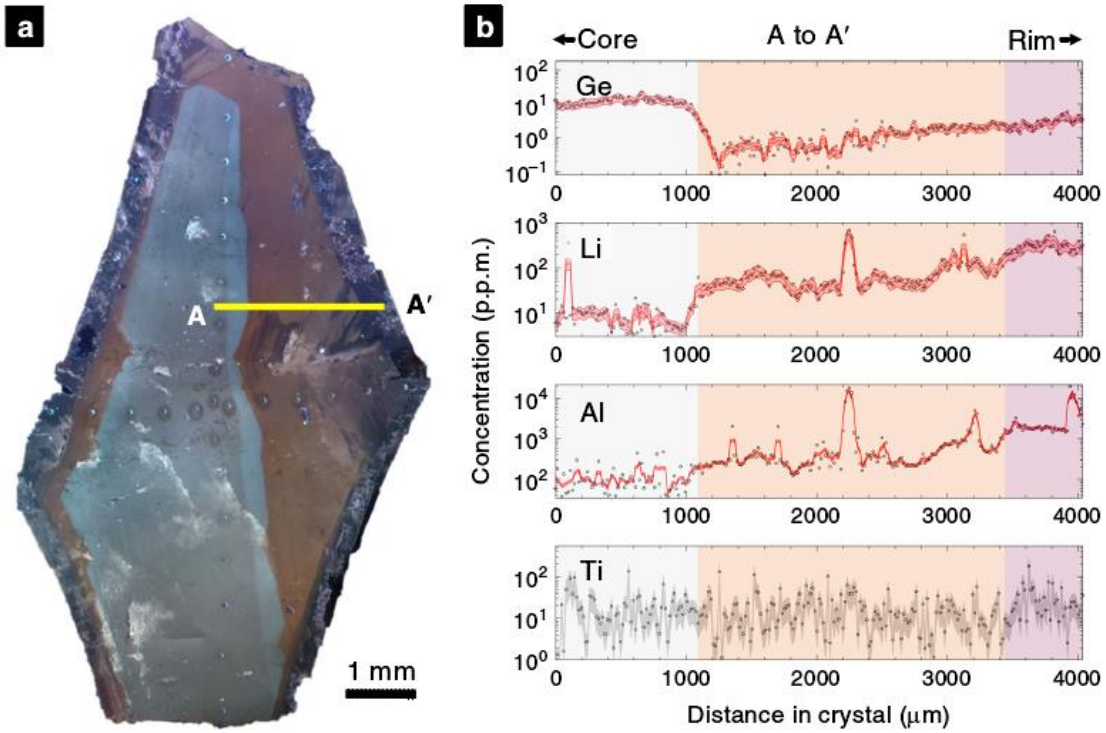

Figure 1. Cathodoluminescence image of a quartz crystal and corresponding trace element transect. a Cathodoluminescence (CL) image of a quartz crystal from the Stewart pegmatite. Yellow line represents trace of geochemical transect. The plane of the crystal is part of {1000}. b Geochemical transect A–A′ for Ge, Li, Al, and Ti in p.p.m. by weight. Dots represent data and red lines represent moving averages. Red envelopes represent standard error of the mean based on 3σ of point analyses and a three-point moving average. Gray envelope in Ti represents 1 standard deviation to the data points. The error values are 26%, 28%, 8.5%, and 57% for Ge, Li, Al, and Ti, respectively. Background colors correspond with CL colors in a. Ti is scattered due to measurements being near detection limits.

3. New Caledonia 和新西兰的地层推断始新世澳大利亚-太平洋板块在南太平洋的运动开启

翻译人:李园洁 liyj3@sustech.edu.cn

Dallanave, E., Maurizot, P., Agnini, C., Sutherland, R., Hollis, C. J., Collot, J., et al. ***Eocene (46-44 Ma) onset of Australia‐Pacific plate motion in the southwest Pacific inferred from stratigraphy in New Caledonia and New Zealand [J]. Geochemistry, Geophysics, Geosystems****, 2020. 21, e2019GC008699. https://doi.org/ 10.1029/2019GC008699*

摘要：太平洋板块环路在始新世早期到中期经历了一个复杂的重组过程，与沿着西太平洋边缘的俯冲开始时间一致。但是西南太平洋的这种变化和 Tonga-Kermadec 岛弧下的俯冲的时间和动力学过程仍不清楚。本文作者从 New Caledonia 的 Koumac-Gomen 地区出露的始新世早期到中期的沉积层得到磁性-生物地层数据。260 m 厚的序列包含深海泥晶灰岩到陆源丰富的钙质浊积岩的过渡，这代表着从稳定的海底高原沉积到汇聚构造域下发展形成的大陆坡。深海泥晶灰岩与上覆钙质浊积岩的地层接触面没有出露。但是基于地磁极性的年代学将过渡带的年龄确定为 46-44 Ma，与 New Caledonia 南部 Noumea 地区得到的 45.3 Ma 一致。作者综合 New Caledonia 的记录和新西兰 South Island 最近的磁性地层数据，这个地区标志着始新世早期和中期陆源输入的变化。西南太平洋同步的沉积物变化发生的时间与澳大利亚和新西兰南部海底快速扩张的时间一致，因此推断地层发生变化的潜在原因是在澳大利亚-太平洋板块边界新格局处开始发生滑动，之后演化成 Tonga-Kermadec 俯冲系统。

ABSTRACT：The Pacific plate circuit went through a complex reorganization during the early to middle Eocene, approximately coinciding with the onset of subduction along the western Pacific margin. However, the timing and dynamics of this change in the southwest Pacific and evolution of subduction beneath the Tonga-Kermadec Arc are not fully resolved. We present magneto-biostratigraphic data from an early to middle Eocene sedimentary section exposed in the Koumac-Gomen area, New Caledonia, which is an emerged portion of the Norfolk Ridge. The 260 m-thick succession contains a transition from pelagic micrite to terrigenous-rich calciturbidite that is observed regionally in New Caledonia and which is interpreted to represent a shift from sedimentation on a stable submarine plateau to slope formation developed under a convergent tectonic regime. The stratigraphic contact between pelagic micrite and overlying calciturbidite is not exposed, but our magnetic polarity-based chronology constrains the age of transition to 46-44

Ma, in agreement with the 45.3 Ma age recently obtained from the Noumea area in southern New Caledonia. We integrate records from New Caledonia with recent magnetostratigraphic data from South Island, New Zealand, where marked variations in terrigenous input occurred during the early and middle Eocene. Synchronous sedimentary changes in the southwest Pacific occurred at the same time as onset of rapid seafloor spreading south of Australia and New Zealand. We infer that the underlying cause of stratigraphic change was inception of slip at a new configuration of the Australia-Pacific plate boundary, which evolved into the Tonga-Kermadec subduction system.

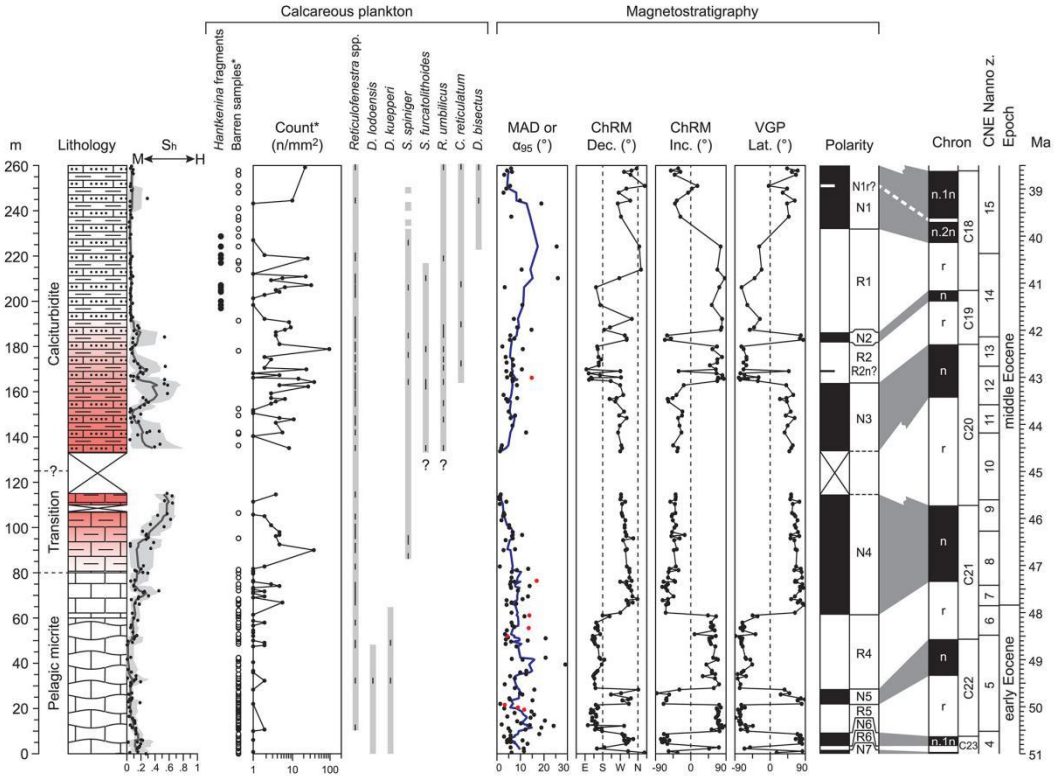

Figure 1. Magneto-biostratigraphy of the Sommet-Khian section. From left to right: Lithology column; the color of the sediment mirrors the amount of high magnetic coercivity hematite as derived by rock - magnetic analyses and Sh parameter (M = magnetite, H = hematite; the 5-point moving average Sh and associated 95% confidence boundaries are estimated following Heslop, 2009); distribution of selected taxa of calcareous plankton; (*) barren samples and count refer to calcareous nannofossil, which abundance is reported on a logarithmic scale as number of specimens (n) per mm2; presence of selected calcareous nannofossil taxa, black lines mark the presence of taxa in the study samples, while the gray bands are the expected stratigraphic ranges from literature (see the text for details); MAD = maximum angular deviation of the characteristic remanent magnetization (ChRM) directions (Kirschvink, 1980) shown together with the 5-point moving average (blue line); red dots are confidence boundary expressed as α 95 (R. Fisher, 1953); ChRM Dec. and Inc. = declination and inclination of each ChRM directions after correction for bedding tilt; VGP Lat. = latitude of the virtual geomagnetic pole associated to each ChRM direction with respect the average paleomagnetic north pole; 0° latitude crossing points are used

to determine the reversals position; the series of normal and reverse magnetic polarity zones has been named as described in the text; question marks indicate zones based on single ChRM directions; geomagnetic polarity time scale (GPTS; Ogg, 2012) shown with the reference calcareous nannofossils zonation (Agnini et al., 2014).

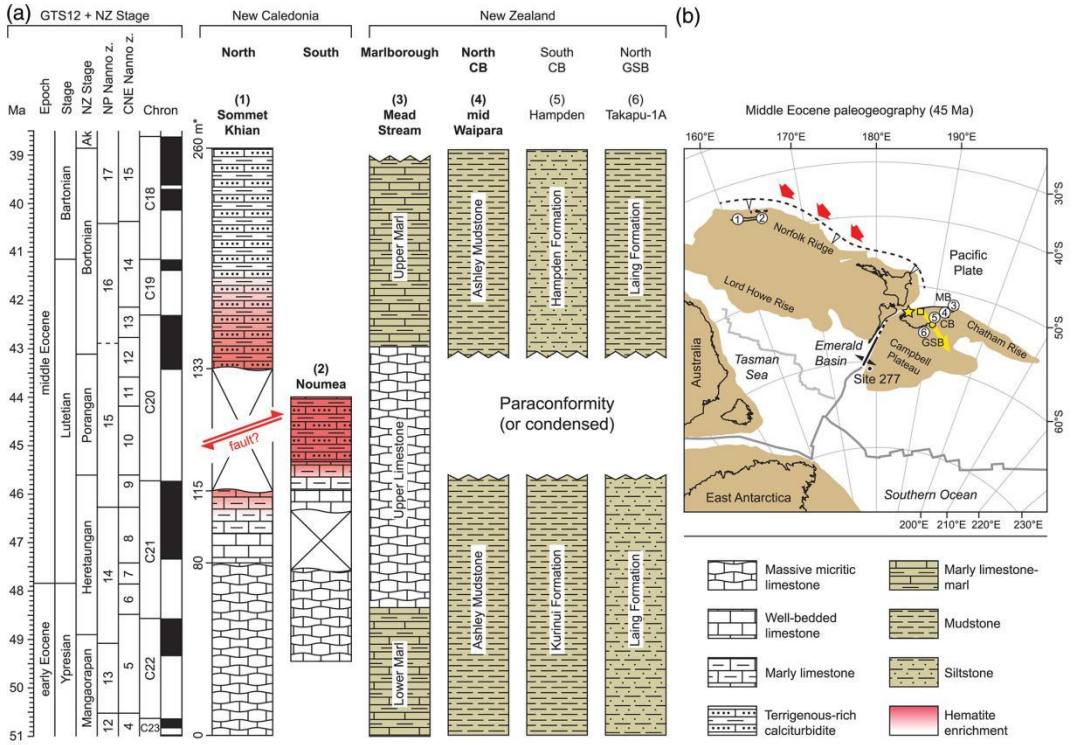

Figure 2. Early-middle Eocene stratigraphy and paleogeography of the Southwest Pacifific area. (a) Magneto-biochronological framework of the sections discussed in the text, from the New Caledonia and the New Zealand areas; the main lithological features are plotted against the international and the New Zealand stages (Gradstein et al., 2012; Raine et al., 2015; Ak = Kaiatan stage), the calcareous nannofossil zonation of Martini (1971; NP zones) and Agnini et al. (2014; CNE zones), and the geomagnetic polarity time scale (GPTS; Ogg, 2012). Sections with magnetic polarity chronology are indicated with the bold font. (b) Paleogeographic reconstruction of the Southwest Pacifific area in the middle Eocene (~45 Ma); continental areas are fifilled in light brown; dotted black line approximates the position of the proto-Tonga-Kermadec subduction zone; the light gray line is the Tasman Ocean spreading ridge, which activity ended during Chron 24n (~53 Ma); and the dark gray lines are active spreading ridges; red arrows indicate the pacifific plate motion relative to the Norfolk ridge, while the yellow star approximate the position of the instantaneous rotational pole of the Pacifific plate with respect the Australian-Lord Howe Rise-Norfolk ridge continental crust at 40-45 Ma; the motion of the pole in the ensuing 10 Myr is represented by the yellow square (40-35 Ma) and dot (35-30 Ma) lying on the yellow arrow (Sutherland, 1995); the main present-day coastlines are indicated for clarity, together with the paleogeographic position of the sections discussed in the main text (numbers refer to records shown in panel a). Map generated with GPlates (Müller et al., 2018) using the rotational parameters of Seton et al. (2012); the instantaneous rotational poles of Sutherland (1995) are rotated anchored to the Pacifific plate.

4. 中国首次火星任务天问一号火星轨道磁力仪

翻译人：柳加波

Liu K, Hao X J, Li Y R, et al. ***Mars Orbiter magnetometer of China's First Mars Mission Tianwen-1****[J].* ***Earth and Planetary Physics****, 2020, 4(4): 384-389.*

https://doi.org/10.26464/epp2020058

摘要：火星轨道磁力仪（MOMAG）是天问一号轨道飞行器上的七个科学载荷之一。MOMAG将测量火星及其周围的磁场，以研究火星空间环境以及与太阳风的相互作用。该仪器由两个相同的三轴磁通门磁力传感器组成，它们安装在 3.19 米长的吊杆上，相距约 90 cm。双磁强计的配置将有助于消除航天器平台和有效载荷产生的磁场干扰。传感器由安装在轨道器内部的电箱控制。每个磁力计在动态范围（每轴 10,000 nT）内以 1.19 pT 的分辨率测量周围矢量磁场。两种磁力计都以 128 Hz 的固有频率对周围磁场进行采样，但是将在 1 到 32 Hz 的交替频率的模式中运行以满足遥测分配。

ABSTRACT: As one of the seven scientific payloads on board the Tianwen-1 orbiter, the Mars Orbiter Magnetometer (MOMAG) will measure the magnetic fields of and surrounding Mars to study its space environment and the interaction with the solar wind. The instrument consists of two identical triaxial fluxgate magnetometer sensors, mounted on a 3.19 meter-long boom with a seperation of about 90 cm. The dual-magnetometers configuration will help eliminate the magnetic field interference generated by the spacecraft platform and payloads. The sensors are controlled by an electric box mounted inside the orbiter. Each magnetometer measures the ambient vector magnetic field over a wide dynamic range (to 10,000 nT per axis) with a resolution of 1.19 pT. Both magnetometers sample the ambient magnetic field at an intrinsic frequency of 128 Hz, but will operate in a model with alternating frequency between 1 and 32 Hz to meet telemetry allocations.

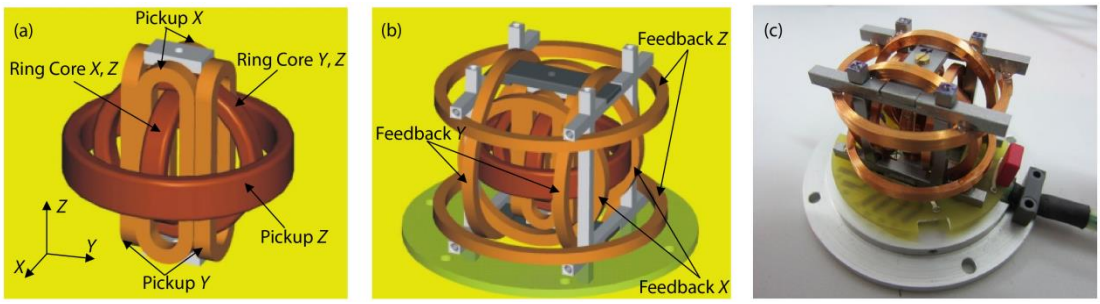

Fig 1. (a, b) Fluxgate magnetometer (FGM) sensor of the 3-D model (Auster et al., 2008). (c) Photograph of an FGM sensor.

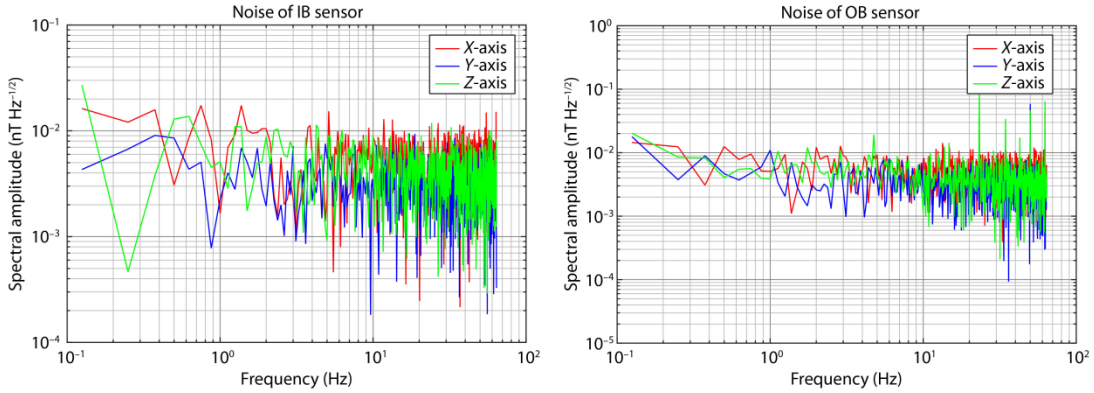

Fig 2. Noise profile of MOMAG sensor as a function of frequencies. IB, inboard; OB, outboard.

5. 近 3000 年来台湾供给到冲绳海槽南部的陆源沉积物不断增加---来自 Sr-Nd 同位素和地球化学的证据

翻译人：刘伟 inewway@163.com

Hu Siyi et al., ***Increasing terrigenous sediment supply from Taiwan to the southern Okinawa Trough over the last 3000 years evidenced by Sr-Nd isotopes and geochemistry*** *[J].* ***Sedimentary Geology****, 2020. https://doi.org/10.1016/j.sedgeo.2020.105725*

摘要：高分辨率的沉积记录能揭示由于气候变化、环境变化和人类活动引起的风化和侵蚀模式。在此，我们通过冲绳海槽南部一个相对高分辨率的沉积记录中硅质沉积物的主量元素、微量元素、Sr-Nd 同位素和沉积堆积率(MARs)，揭示了台湾的源-汇沉积过程、物理侵蚀和化学风化历史。Sr-Nd 同位素资料表明，沉积物主要来源于台湾东北部和西部河流，因而能记录反映了该源区的风化剥蚀状况。自约 3000 年以来，中国大陆和台湾东部的火山岩、风尘和陆源河流沉积物对冲绳海槽南部沉积物的贡献不大。利用化学风化指数(CIA)、K/Al, α^{Al}K, Ti/Na, and K/Na 等多种指标来识别区域尺度的化学风化强度变化。利用硅质碎屑的 MAR(siliciclastic)和 Ti 的 MAR(Ti)来估算沉积物输入的强度。结果表明，自约 3000 年以来，台湾山地河流系统的基岩经历了相对稳定和适度的化学风化，台湾向冲绳海槽南部的陆源沉积物供应逐渐增加。将这些资料与气候及人类活动比较后发现，陆源沉积物输入的增加与台湾近三千年来降雨量的增加密切相关。大约 1500 年之后，陆源沉积物输入持续增加，这可能是强降雨和人类活动共同作用的结果。台湾河流盆地强烈的物理侵蚀对化学风化强度产生了长期的制约作用。在这些流域中，硅酸盐风化与气候强迫之间缺乏明显的联系，这表明基于台湾河流近海沉积地球化学记录的古气候重建需要慎重考虑。

ABSTRACT: High-resolution sedimentary records reveal the patterns of weathering and erosion in response to climate change, environmental variability, and human activity. Here, we present major and trace element data, Srsingle bondNd isotopic compositions, and mass accumulation rates (MARs) for the siliciclastic sediment fraction of a relatively high-resolution sedimentary archive from the southern Okinawa Trough, East China Sea. We reveal the sedimentary source-to-sink processes and the physical erosion and chemical weathering history of Taiwan. The Sr-Nd isotopic data indicate that sediments were mainly sourced from northeastern and western Taiwan rivers and

thus, the sedimentary records reflect the weathering and erosion conditions in this source region. Volcanic rocks, aeolian dust, and terrigenous sediment from rivers in mainland China and eastern Taiwan have not significantly contributed to the deposits in the southern Okinawa Trough since ca. 3000 cal yr BP. Multiple indices, including the chemical index of alteration (CIA), K/Al, $\alpha^{Al}K$, Ti/Na, and K/Na, are used to identify variations in the intensity of regional-scale chemical weathering. The strength of the sediment input is estimated using the MAR of the siliciclastic (MARsiliciclastic) and the MAR of Ti (MARTi). The results suggest that the bedrock of small mountainous river systems in Taiwan has experienced relatively stable and moderate chemical alteration and that the terrigenous sediment supply from Taiwan to the southern Okinawa Trough has progressively increased since ca. 3000 cal yr BP. A comparison of these data with climate and human activity indicates that the increased input of terrigenous sediment was closely related to an intensification of rainfall in Taiwan over the last 3000 years. After ca. 1500 cal yr BP, a sustained increase in the terrigenous sediment input likely to be attributed to the combined effects of intensified heavy rainfall and human activity, occurred. Intense physical erosion in Taiwan's river basins has exerted a long-term constraint on chemical weathering intensity. The lack of evident link between silicate weathering and climate forcing in these catchments suggests that paleoclimate reconstruction based on sedimentary geochemical records offshore of Taiwan rivers requires careful consideration.

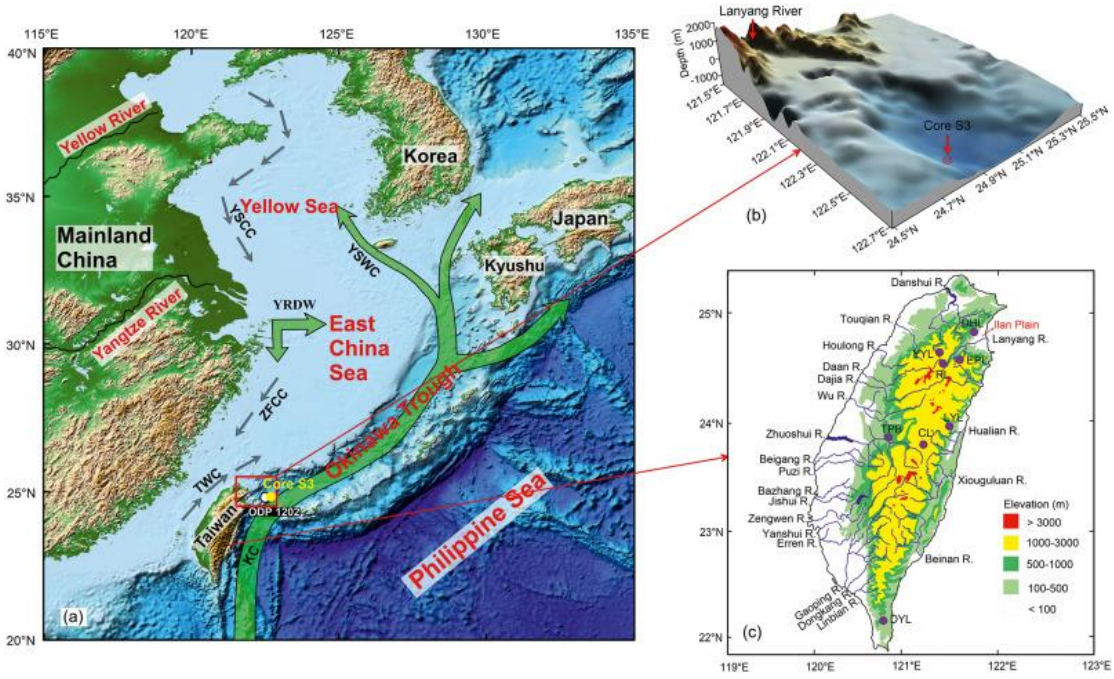

Figure 1. Map of the study area showing the location of Core S3 (a), the topography of the southern Okinawa Trough (b), and the major hydrographic network of Taiwan modified from Milliman and Farnsworth (2011) (c).

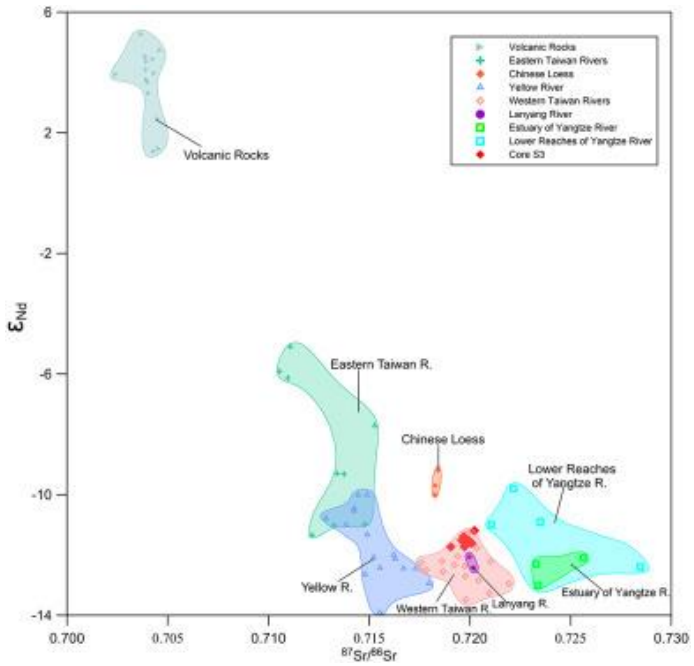

Figure 2. Sediment provenance discrimination diagram of $^{87}Sr/^{86}Sr$ versus ε_{Nd}. Sr-Nd isotopic data for volcanic rocks in the Okinawa Trough from (Shinjo et al., 1999), Chinese loess silicate (Chen et al., 2007), Yangtze River and Yellow River sediments (Yang et al., 2007; Meng et al., 2008), and Taiwan river sediments (Dou et al., 2016) plotted for comparison. The average isotopic compositions of the potential endmembers are shown in Table 3.

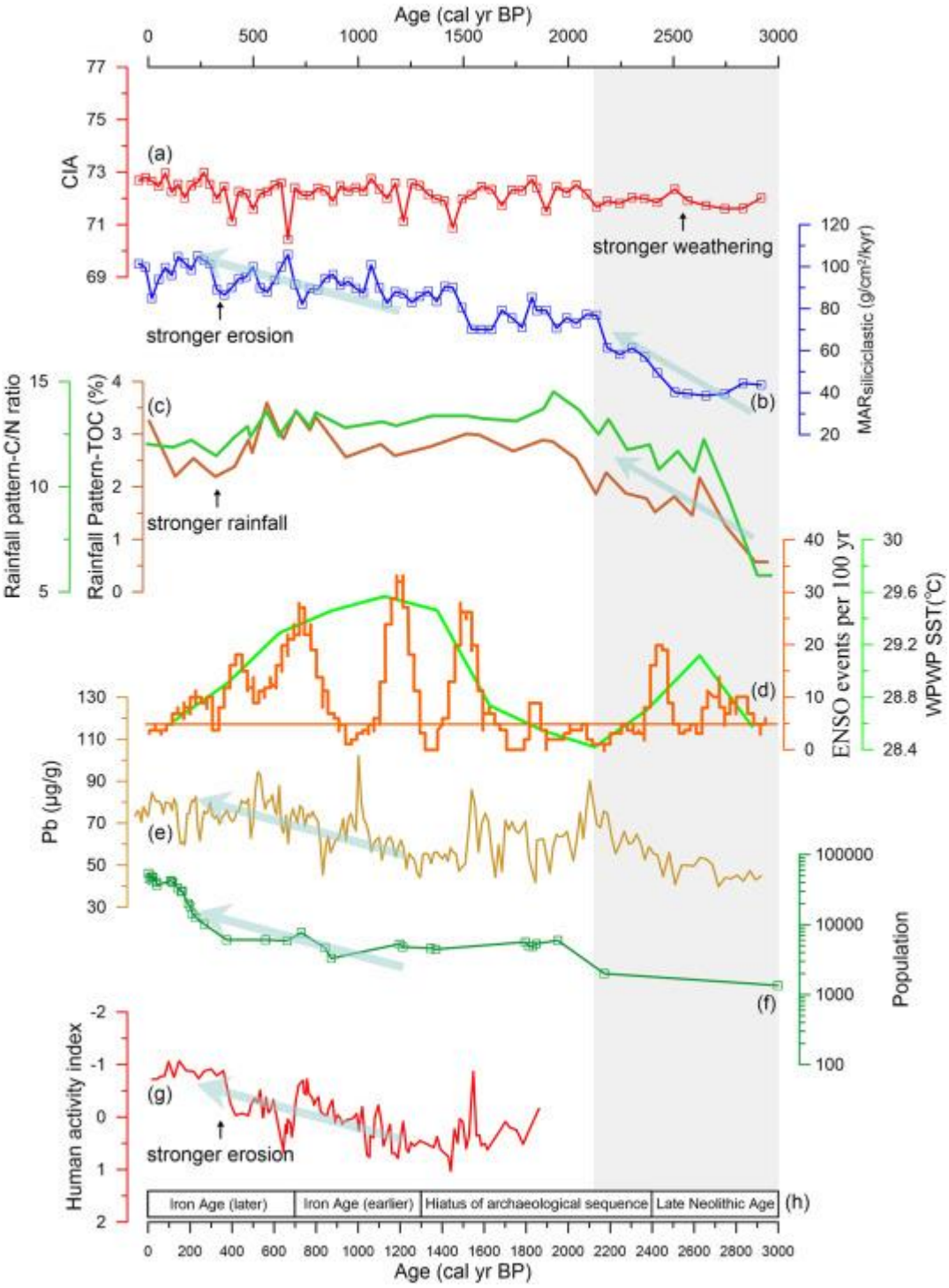

Figure 3. Comparison of the Core S3 records with other representative paleoclimate, human activity, and archeological evidence from Taiwan and human population changes in China (logarithm with base 10) since 3000 cal yr BP: (a) CIA values from Core S3; (b) $MAR_{siliciclastic}$ values from Core S3; (c) reconstructed rainfall pattern for Taiwan from the Emerald Peak Lake record (Selvaraj et al., 2012; Wang et al., 2015); (d) El Niño/Southern Oscillation (ENSO) intensity from Ecuador (Moy et al., 2002) and sea surface temperature (SST) of the Western Pacific Warm Pool (WPWP) (Stott et al., 2004); (e) Pb concentrations from Core S3; (f) human population change in China; (g) pollen-based human activity index for Taiwan(Wang et al., 2014b); and (h) the archeological sequence from northeastern Taiwan (Lin et al., 2007).

6. 印度-西藏碰撞带的印度下地壳局部塌陷

翻译人：曹伟 11930854@QQ.com

Shi D., Klemperer S.L., Shi J.Y., et al. ***Localized foundering of Indian lower crust in the India–Tibet collision zone*** *[J].* ***PNAS****. 2020:10:16019*

https://doi.org/10.1038/s41598-020-72849-z

摘要：印度与亚洲大陆碰撞的深部构造，以及印度的下地壳是在西藏之下还是俯冲到地幔中，仍然存在争议。目前还不清楚是造成西藏上地壳造山带平行伸展的活跃正断层是继续延伸到下地壳还是上地幔。我们采集的与印度-西藏碰撞带平行的接收函数图像显示，在(88.5°-92°E）雅鲁-藏布缝合带之下，厚度为 20 公里的印度下地壳，在 Cona-Sangri 和 pumquo-xainza 断裂带附近基本上不存在，这表明上地壳和下地壳减薄之间存在明显联系。与印度下地壳厚度共变的卫星重力数据与 30%榴辉岩化下地壳相一致，因此重力稳定。莫霍面偏移和局部榴辉岩化的印度下地壳横向减薄与深地震结果吻合，这表明印度下地壳正在局部下沉或停止进入地幔。印度下地壳的这种亏损意味着重力不稳定，这可能是由于弱水镁铁质花岗岩的脱水反应或两个地堑下直接的挥发性软流上升流所导致的局部快速榴辉岩化。我们认为碰撞带下同时存在着两种相互竞争的过程，一种是由底侵作用的高原形成，另一种是由下沉或顶蚀作用造成的大陆损失。

ABSTRACT: The deep structure of the continental collision between India and Asia and whether India s lower crust is underplated beneath Tibet or subducted into the mantle remain controversial. It is also unknown whether the active normal faults that facilitate orogenparallel extension of Tibetan upper crust continue into the lower crust and upper mantle. Our receiver-function images collected parallel to the India Tibet collision zone show the 20-km-thick Indian lower crust that underplates Tibet at 88.5-92°E beneath the Yarlung-Zangbo suture is essentially absent in the vicinity of the Cona-Sangri and Pumqu-Xainza grabens, demonstrating a clear link between upper-crustal and lower-crustal thinning. Satellite gravity data that covary with the thickness of Indian lower crust are consistent with the lower crust being only 30% eclogitized so gravitationally stable. Deep earthquakes coincide with Moho offsets and with lateral thinning of the Indian lower crust near the bottom of the partially eclogitized Indian lower crust, suggesting the Indian lower crust is

locally foundering or stoping into the mantle. Loss of Indian lower crust by these means implies gravitational instability that can result from localized rapid eclogitization enabled by dehydration reactions in weakly hydrous mafic granulites or by volatilerich asthenospheric upwelling directly beneath the two grabens. We propose that two competing processes, plateau formation by underplating and continental loss by foundering or stoping, are simultaneously operating beneath the collision zone

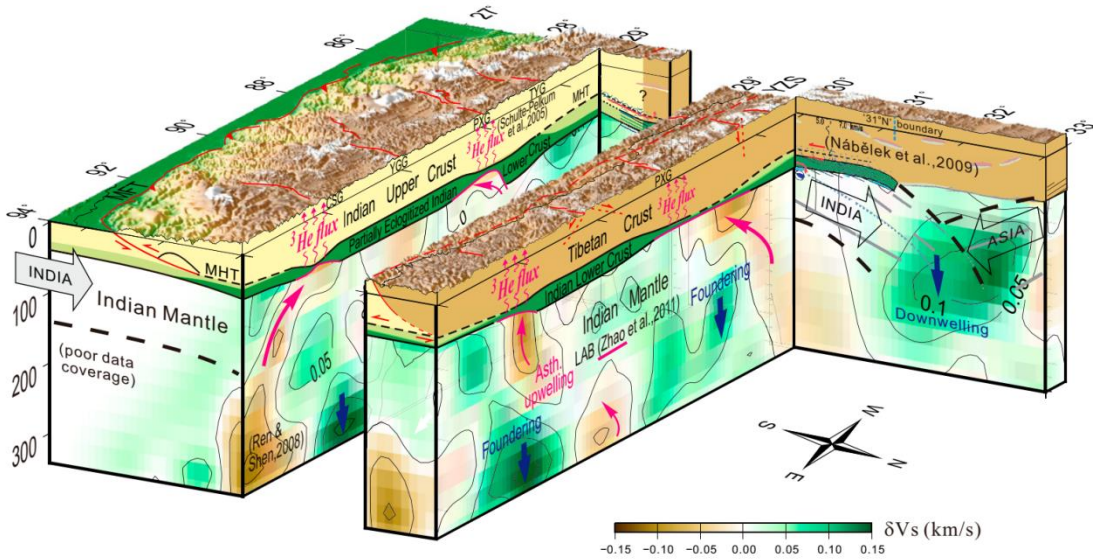

Figure 1. Interpretive cartoon (with exaggerated topography) of processes currently operating in the India–Tibet collision zone. Beneath the Moho we show mantle S-wave velocity structure from our teleseismic tomography (SI Appendix, Figs. S6 and S8). ILC is simultaneously underplating and foundering beneath the CSG and PXG grabens, and foundering then subducting at the northern end of the collision zone. West–east cuts in the three-dimensional block model are along our Profiles A and B. South–north cut along 85°E from ref. 7. Arrows are inferred directions of lithospheric foundering (dark blue) and asthenospheric upwelling (purple) in the upper mantle.

7. 利用硅藻和沉积物中湖相有机物的稳定同位素组成揭示喜马拉雅中部在 MIS 3 晚期的古环境

翻译人：杨会会 11849590@mail.sustech.edu.cn

Rahman A, Sarkar S, Kumar S et al., ***Paleoenvironment of the Central Himalaya during late MIS 3 using stable isotopic compositions of lacustrine organic matter occluded in diatoms and sediments*** *[J].**Quaternary International**, 2020,558, 1-9.*

https://doi.org/10.1016/j.quaint.2020.08.024

摘要：深海氧同位素阶段 3（MIS3）是地球气候历史上的一个间冰阶，它的最后一个阶段（40-30 ka），相比于世界上的其他地区，在中国西北部，青藏高原，和印度东北部表现为相对温暖的气候。然而，关于这一时期喜马拉雅地区气候变化的研究报告并不多。本文中，我们试图利用碳同位素（$\delta^{13}C_{TOC}$）和氮同位素（$\delta^{15}N_{TN}$）组成，还有他们在古湖泊序列中块状有机物的的元素比值（TOC/TN）和硅藻细胞膜中封存的有机物的同位素（$\delta^{13}C_{Diatom}$），来研究喜马拉雅中部在 45-29 ka 的古环境变化。$\delta^{13}C_{Diatom}$，$\delta^{13}C_{TOC}$ 和 TOC/TN 的变化指示了湖泊碳动力从重碳酸盐主导体系到二氧化碳主导体系的间歇性变化。湖相碳循环的这些变化为喜马拉雅中部在 45-29 ka 期间存在的少数干旱事件提供了证据。与中国西北部，青藏高原和印度西北部的记录一致，我们的结果也确认了喜马拉雅中部在 40-32 ka 期间气候较为湿润。因此，因此，与世界其他地区相比，这一地区的气候似乎较为湿润。然而，这一湿润阶段背后的机制仍有待探索，需要在喜马拉雅山进行高分辨率的古气候研究。

Abstract: Marine Isotope Stage (MIS) 3 was an interstadial stage in the climate history of the Earth where the last phase (40-30 ka) showed relatively warmer climate over the northwest China, Tibetan Plateau, and northwestern India compared to other regions of the world. However, not many studies are reported for climate variability during this period from the Himalayan region. Here, an attempt has been made to understand the paleoenvironment of the Central Himalaya during 45-29 ka using stable isotopic compositions of carbon ($\delta^{13}C_{TOC}$) and nitrogen ($\delta^{15}N_{TN}$) along with their elemental ratios (TOC/TN) in bulk organic matter and occluded organic matter within diatom frustules ($\delta^{13}C_{Diatom}$) of a paleolake sequence. The variabilities in $\delta^{13}C_{Diatom}$, $\delta^{13}C_{TOC}$, and TOC/TN ratios indicated intermittent changes in the lake carbon dynamics from bicarbonate dominated system to

carbon dioxide dominated regime. These changes in lacustrine carbon cycling provided evidence for existence of sporadic dry events in the Central Himalaya during 45-29 ka. In agreement with the records from the northwest China, Tibetan Plateau, and northwestern India, our results also confirm the existence of a relatively wet and humid period during 40-32 ka in the Central Himalaya. Therefore, it appeared that compared to other parts of the world, relatively wet and humid climate existed throughout this region. However, the mechanism behind this wet and humid phase remains to be explored and warrants a high resolution paleoclimate study in the Himalaya.

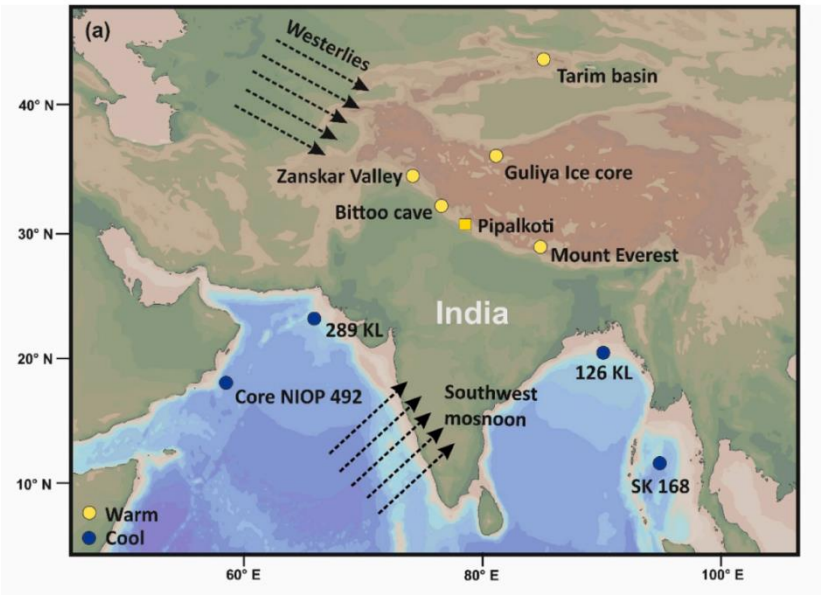

Figure 1. Schematic diagram showing (a) location of the study area (square) and (b) detailed map of the basin in which study area is located. Locations of the previous studies covering time period 40 to 30 ka in the region are also shown (Zanskar valley: Chahal et al. (2019); Bittoo cave: Kathayat et al. (2016); Tarim basin: Yang et al. (2004); Yang et al. (2006); Mount Everest: Finkel et al. (2003); Guliya ice core: Thompson et al. (1997), Core NIOP 492: Reichart et al. (1998); 289 KL: Deplazes et al. (2014); 126 KL: Kudrass et al. (2001); SK168: Kumar et al. (2018). Yellow circles in (a) represent studies advocating wet period during 40-30 ka and blue circles represent studies supporting weak Indian summer monsoon during late MIS 3. (For interpretation of the references to color in this figure legend, the reader is referred to the Web version of this article.)

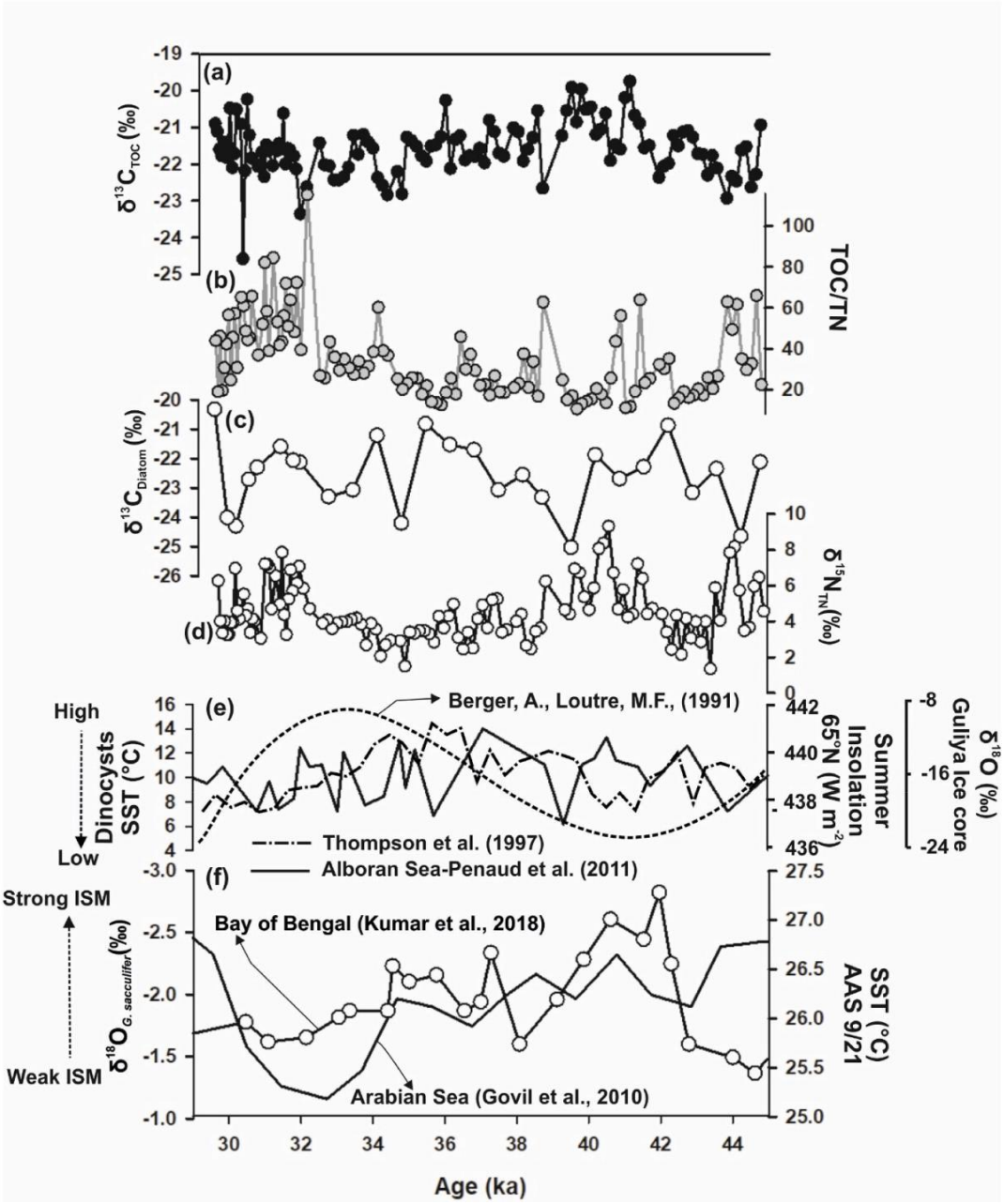

Figure 2. Results of the present study in comparison with various other regional and global studies (a) carbon isotopic compositions of organic matter ($\delta^{13}C_{TOC}$), (b) TOC/TN ratios, (c) carbon isotopic compositions of occluded organic matter within diatom ($\delta^{13}C_{diatom}$), (d) nitrogen isotopic compositions of bulk sediments ($\delta^{15}N_{TN}$), (e) Alboran Sea-Dinocyst SST (°C) - solid line; Guliya ice core $\delta^{18}O$ - dashed-dotted line; NH summer insolation (65°N) - dotted line, and (f) the Bay of Bengal marine core-$\delta^{18}O_{G.sacculifer}$ - solid line with circles; Arabian Sea AAS 9/21-SST (°C)- solid line.

8. 沙漠粉尘、海洋生物地球化学和气候之间的全球铁联系

翻译人：王敦繁 dunfan-w@foxmail.com

Jickells, T. D. ***Global Iron Connections Between Desert Dust, Ocean Biogeochemistry, and Climate[J]****.* ***Science****, 2005, 308(5718):67-71.* Doi: 10.1126/science.1105959

摘要：地球的环境条件，包括气候，是由物理、化学、生物和人类相互作用决定的，这些相互作用转化和运输物质和能源。这就是“地球系统”:一个高度复杂的实体，具有多个非线性响应和阈值，不同的部件之间存在联系。这个系统的一个重要部分是铁循环，在这个循环中，含铁的土壤尘埃从陆地通过大气转移到海洋，影响海洋生物地球化学，从而对气候和尘埃产生反馈作用。这里我们回顾了这个周期的关键组成部分，确定了未来研究的关键不确定性和优先级。

ABSTRACT: The environmental conditions of Earth, including the climate, are determined by physical, chemical, biological, and human interactions that transform and transport materials and energy. This is the ‘‘Earth system’’: a highly complex entity characterized by multiple nonlinear responses and thresholds, with linkages between disparate components. One important part of this system is the iron cycle, in which iron- containing soil dust is transported from land through the atmosphere to the oceans, affecting ocean biogeochemistry and hence having feedback effects on climate and dust production. Here we review the key components of this cycle, identifying critical uncertainties and priorities for future research.

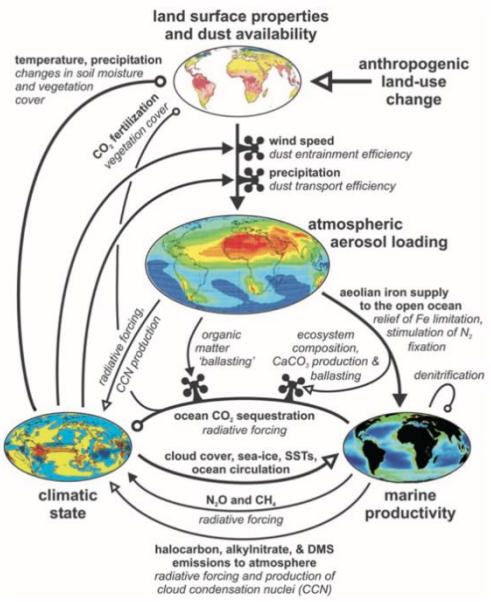

Figure 1. Schematic view of global iron and dust connections. Highlighted are the four critical components (clockwise from top): the state of the land surface and dust availability, atmospheric aerosol loading, marine productivity, and some measure of climatic state (such as mean global surface temperature). The sign of the connections linking these varies; where the correlation is positive (for example, increased atmospheric aerosol loading Y increased marine productivity), the line is terminated with a solid arrowhead. Where the correlation is negative (for example, increased marine productivity Y lower CO_2 and a colder climate), the termination is an open circle. Connections with an uncertain sign are terminated with an open arrowhead. The mechanism by which the link acts (for example, the impact of a change in atmospheric CO_2 is via the radiative forcing of climate) is displayed in italics. Finally, the ‘‘water tap’’ symbols represent a secondary mechanism modulating the effect of a primary mechanism; for instance, a change in global precipitation strength and distribution will alter the efficiency with which entrained dust is transported to the open ocean. If a path of successive connections can be traced from any given component back to itself, a closed or feedback loop is formed. An even number (including zero) of negatively correlated connections counted around the loop gives a positive feedback, which will act to amplify a perturbation and tend to destabilize the system. Conversely, an odd number of negative correlations gives a negative feedback, dampening any perturbation and thus stabilizing the system. For instance, atmospheric aerosol loading Y marine productivity Y climatic state Y dust availability Y atmospheric aerosol loading contains two negative and two positive correlations and thus is positive overall. In contrast, marine productivity looping back onto itself contains a single negative correlation and thus represents a negative feedback.

9. 全新世以来死海沉积物的磁学性质能够作为区域性水文气候监测手段

翻译人：王浩森 11930841@mail.sustech.edu.cn

Ebert Y, Shaar R, Levy E J, et al. ***Magnetic properties of late Holocene Dead Sea sediments as a monitor of regional hydroclimate[J].Geochemistry,Geophysics,Geosystems,*** *2020.*

https://doi.org/10.1029/2020GC009176

摘要：缺氧沉积环境中的成岩作用主要通过碎屑磁铁矿的溶解和自生钙镁矿的沉淀来影响沉积物的磁性。最新得到的晚全新世时期的死海沉积物提供了机会，可以研究控制钙锌矿形成和保存的过程，以及它们与不同水文环境之间的关系。磁数据和孔隙流体成分是从死海西部沿 N-S 断面的三个全新世剖面获得的：Og，Ein-Feshkha 和 Ein-Gedi。北部靠近死海的主要淡水源-约旦河。碎屑钛磁铁矿存在于以上所有断面，但在 Og 和 Ein-Feshkha 处，辉绿岩是主要的载磁矿物。块体之间和块体内的块状岩石磁数据变化超过三个数量级，其中较高的值表示较高的钙铁矿浓度。在这三个位置，孔隙流体的盐度与现代和全新世的死海盐水相似或更低，具有可变的和溶解的铁（Fe^{2+}）和硫酸盐（SO_4^{2-}）。磁性的变化反映在铁和/或硫酸盐微生物的还原作用下，该还原作用可控制沉积物中钙锌矿的形成。我们认为，N-S 钙铁矿的减少表明缺氧微生物的活性是由不稳定的有机物和/或反应性铁所控制的，这些有机物和/或反应性铁是由约旦河的淡水涌入而引起或形成的。因此，钙铁矿的浓度变化取决于过去向高盐湖输入的淡水以及与淡水源的距离。水文条件与磁性之间的表观关系提供了一种追踪死海过去水文变化的新方法。

ABSTRACT: Diagenetic processes in anoxic sedimentary environments influence sediment magnetic properties mainly through dissolution of detrital magnetite and precipitation of authigenic greigite. Recently exposed late Holocene Dead Sea sediments provide an opportunity to study the processes governing greigite formation and preservation, and their relation to different hydrological settings. Magnetic data and pore-fluid compositions were obtained from three Holocene sections along a N-S transect on the western Dead Sea shore: Og, Ein-Feshkha, and Ein-Gedi. The northern sections are closer to the major freshwater source to the Dead Sea – the Jordan River. Detrital titanomagnetite is present at all sections, but greigite is the dominant magnetic phase at Og and Ein-Feshkha. Bulk rock magnetic data varies between and within the sections by over three orders of

magnitude, where higher values indicate higher greigite concentrations. At the three sites, pore-fluids have similar or lower salinity than the modern and Holocene Dead Sea brine, with variable and dissolved iron (Fe^{2+}) and sulfate (SO_4^{2-}). Magnetic property changes are reflected by iron and/or sulfate microbial reduction that controlled sedimentary greigite formation. We propose that the N-S greigite decrease suggests that anoxic microbial activity was controlled by labile organic matter and/or reactive iron brought by, or formed as a result of, freshwater influx from the Jordan River. Hence, greigite concentration changes depended on past freshwater input to the hypersaline lake and proximity to the freshwater source. The apparent relationship between hydrological conditions and magnetic properties provides a new method to trace past hydrological changes in the Dead Sea.

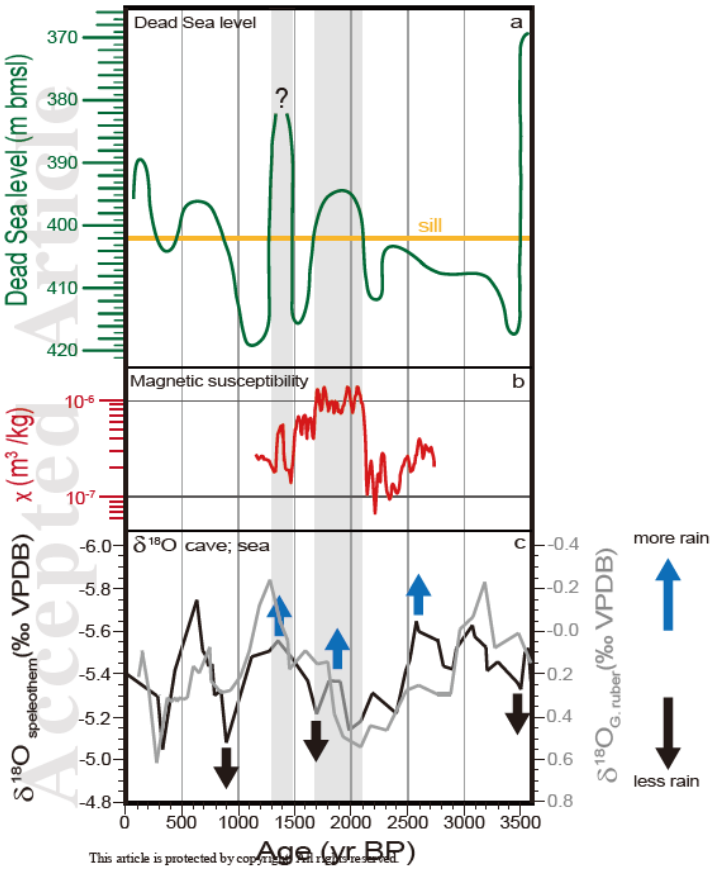

Figure 1. (a) Dead Sea lake level for the past 3500 yr BP (after Bookman et al. (2004); Migowski et al. (2006), and Kushnir & Stein (2019)). The yellow line marks the sill level (402 m bmsl), which is a natural barrier that separates the northern, deeper lake from the shallow southern part. Gray shading marks the association between lake levels above the sill and higher χ. (b) Smoothed (running average) χ profile for the Ein-Feshkha section. (c) $\delta^{18}O$ from an Eastern Mediterranean deep-sea core (foraminiferal data from Schilman et al. (2001)) and in a Soreq Cave speleothem (after Schilman et al. (2002)). The overall $\delta^{18}O$ pattern in the Soreq Cave speleothem (calcite) resembles that of foraminiferal $\delta^{18}O$ (reflecting Eastern Mediterranean seawater values). Nevertheless, variations in the amplitudes of $\delta^{18}O$ in the sea and the cave (expressed by $\Delta^{18}O_{cave\text{-}sea}$ values; see Suppl. Fig. S3) are related to the amount effect in the vicinity of the cave in the Judean Mountains. At 1.4 ka, the sea-cave difference reflects enhanced inflow of low- $\delta^{18}O$ Nile River water to the Eastern Mediterranean. Correlation between lake level, χ, and $\delta^{18}O$ values is evident, where high χ corresponds to high lake levels that reflect mainly increased Jordan River freshwater inputs. See text for discussion of the figure and its implications.

10. 水下洞穴的 Mg 元素作为潜在的古温度指标

翻译人：郑威　11930589@mail.sustech.edu.cn

Drysdale R, Couchoud I, Zanchetta G, et al. ***Magnesium in subaqueous speleothems as a potential palaeotemperature proxy****[J].* ***Nature Communications****, 2020, 11(1): 1-11.*

https://doi.org/10.1038/s41467-020-18083-7

摘要：极地地区之外鲜有能保存跨越多个冰期间冰期旋回的连续的可定年的古温度代用指标时间序列。这阻碍了构建更完善的全球温度变化图景。在这里我们展示了一个意大利水下洞穴沉积物的Mg元素浓度变化，它追踪了过去35万年以来的区域海表面温度。Mg元素浓度在暖期较高，冷期时候相反。与早期研究不同的地方是，这表明了Mg元素浓度变化主要受到温度而非降雨的控制。洞穴沉积物的沉积背景导致Mg分配系数比其他方解石更依赖于温度，从而使温度变化对Mg分配的影响远超过水源的Mg/Ca比变化。有相似深部洞穴环境的水下洞穴沉积物应该能提供多个冰期间冰期旋回的古温度信息。

ABSTRACT: Few palaeoclimate archives beyond the polar regions preserve continuous and datable palaeotemperature proxy time series over multiple glacial-interglacial cycles. This hampers efforts to develop a more coherent picture of global patterns of past temperatures. Here we show that Mg concentrations in a subaqueous speleothem from an Italian cave track regional sea-surface temperatures over the last 350,000 years. The Mg shows higher values during warm climate intervals and converse patterns during cold climate stages. In contrast to previous studies, this implicates temperature, not rainfall, as the principal driver of Mg variability. The depositional setting of the speleothem gives rise to Mg partition coefficients that are more temperature dependent than other calcites, enabling the effect of temperature change on Mg partitioning to greatly exceed the effects of changes in source-water Mg/Ca. Subaqueous speleothems from similar deep-cave environments should be capable of providing palaeotemperature information over multiple glacial-interglacial cycles.

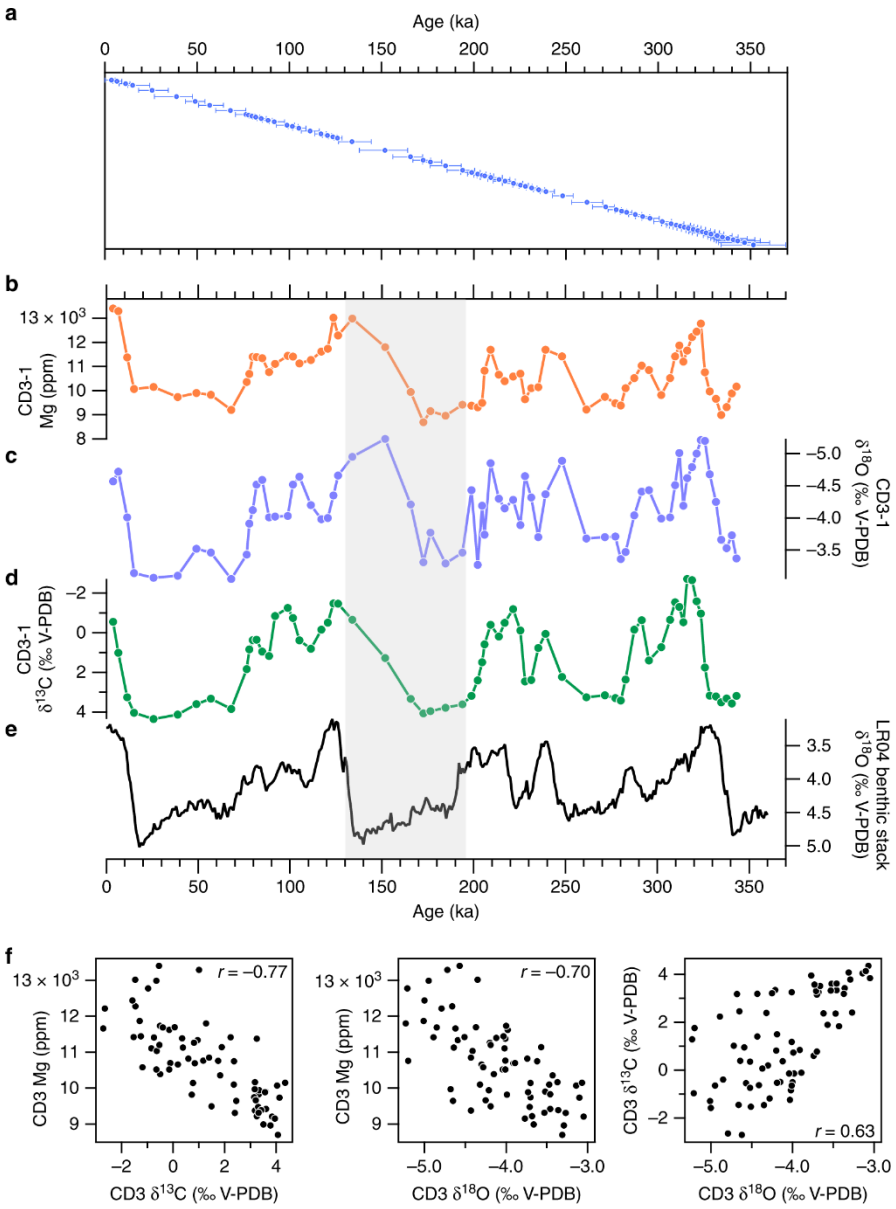

Figure 1. a. The blue circles show the distribution across time of 115 radiometric ages (see Supplementary Data 1) on CD3-1 (see Supplementary Fig. 1 for the age-depth model and the age uncertainty time series). The error bars are 2σ uncertainties based on the U-Th age calculations. **b**–**d.** Mg, $\delta^{18}O$ and $\delta^{13}C$ series from CD3-1 sampled at 1 mm resolution (see 'Methods'). **e** The Lisiecki and Raymo[51]LR04 benthic $\delta^{18}O$ stack. The grey vertical band is the MIS 6-to-Termination II (~195–130 ka) interval where the greatest age discrepancy occurs between the CD3-1 series and the benthic $\delta^{18}O$ (see main text for discussion). **f** Scatterplots and Pearson's *r* correlation coefficients for CD3-1 data shown in **b**–**d**. All *r*-values are statistically significant at $p < 0.05$.

11. 台湾托舍盆地湖相沉积物中全新世晚期的古火、植被与气候重建

翻译人：李海 12031330@mail.sustech.edu.cn

Huang, Z., Ma, C., Chyi, S-.J., Tang, L., & Zhao, L. ***Paleofire, vegetation, and climate reconstructions of the middle to late Holocene from lacustrine sediments of the Toushe Basin, Taiwan[J]****.* ***Geophysical Research Letters****, 2020.47, e2020GL090401.*

https://doi.org/10.1029/2020GL090401

摘要：根据台湾头社盆地的高分辨率加速质谱仪(AMS) ^{14}C 年代沉积物剖面，基于花粉和木炭的浓度，我们确定了此前在 6.2 至 1.3 cal kyr BP 之间的四个气候阶段。从 6.2 到 4.6 cal kyr BP，该地区温暖湿润，很少发生野火，主要是亚热带常绿阔叶林。气候变冷-干燥，从 4.6 到 3.0 cal kyr BP，森林减少，火灾频率增加。在 3.0～2.1 cal kyr BP 时，气候进一步降温干燥，高寒草甸发育，火灾发生频率增加。该地区从 2.1 cal kyr BP 到 1.3 cal kyr BP 变得更加温暖和湿润，伴随着森林的恢复。气候变化与东亚夏季风强度的变化有关，而东亚夏季风强度主要受太阳辐射控制。野火很可能是受东亚夏季季风和厄尔尼诺-南下振荡影响的降水变化所控制的。在厄尔尼诺年间，头社盆地经历了干旱和频繁的野火。

Abstract We identified four climatic stages between 6.2 and 1.3 cal kyr before present (BP) based on pollen and charcoal concentrations by high-resolution Accelerated mass spectrometer (AMS) ^{14}C-dated sediment profile from Taiwan's Toushe Basin. From 6.2 to 4.6 cal kyr BP, the region was warm-wet with infrequent wildfires and dominant subtropical evergreen broad-leaved forests. The climate was cooler-drier from 4.6 to 3.0 cal kyr BP, with a decline in forest and increased fire frequency. From 3.0 to 2.1 cal kyr BP, climate further cooled and dried, with the development of alpine meadows and higher fire frequency. The region became warmer and wetter from 2.1 to 1.3 cal kyr BP, accompanied by forest recovery. Climatic changes were linked to changes in East Asia Summer Monsoon intensity, which is mainly controlled by solar radiation. Wildfires were likely controlled by precipitation variability that is influenced by East Asia Summer Monsoon and El Niño-Southern Oscillation. Toushe Basin experienced drought conditions and frequent wildfires during the El Niño years.

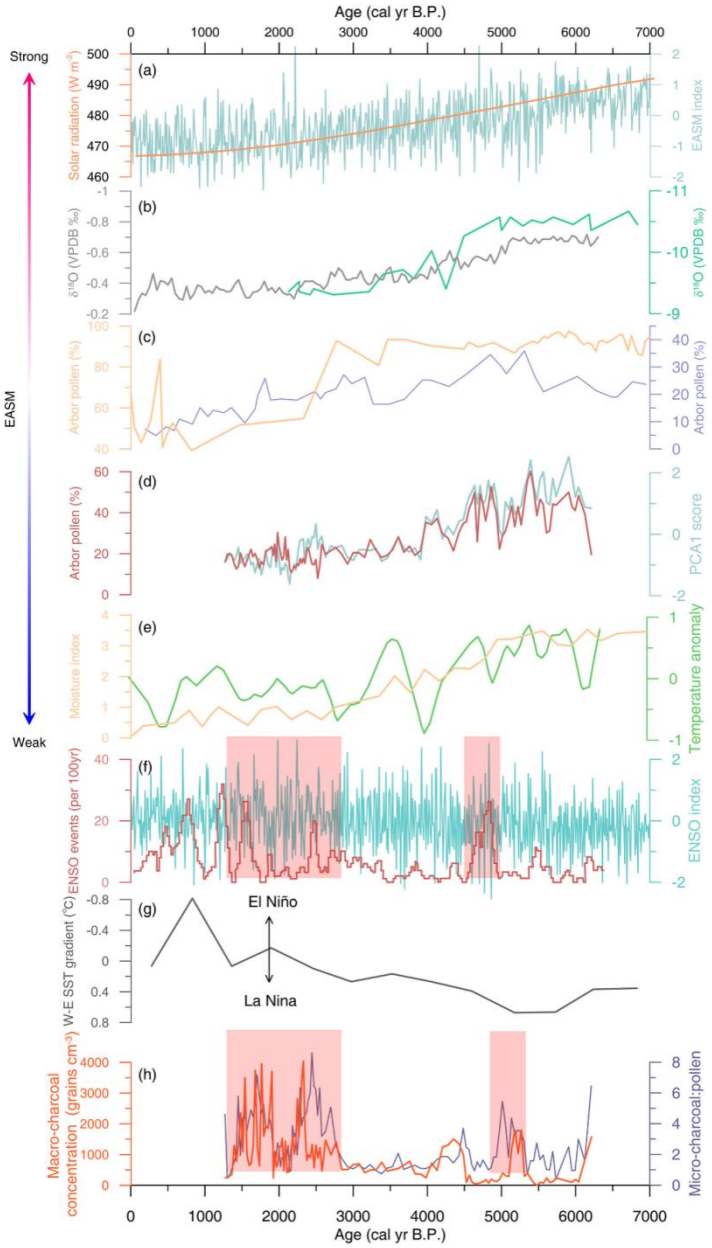

Figure 1. Comparisons between the pollen and charcoal records in the Toushe Basin with nearby paleoclimate records since 6.2 kyr BP, including (a) left, solar radiation in June at 25°N (Berger & Loutre, 1991), and right, reconstructed EASM index (Zhang et al., 2018); (b) left, integrated stalagmite $\delta^{18}O$ record in South China (Yang et al., 2019), and right, stalagmite $\delta^{18}O$ record in Sanbao Cave (Dong et al., 2010); (c) left, arboreal pollen percentage in Daiyunshan (Zhao et al., 2017), and right, arboreal pollen percentage in Huguanyan maar lake (Wang et al., 2007); (d) left, arboreal pollen percentage in the Toushe Basin (this study), and right, the PCA1 scores of the pollen record in the Toushe Basin (this study); (e) left, precipitation index in southern China (Ran & Feng, 2013), and right, reconstructed temperature anomaly in China (Fang & Hou, 2011); (f) left, ENSO frequency near the equator (Moy et al., 2002), and right, reconstructed ENSO index (Zhang et al., 2018); (g) west to east Pacific sea surface temperature (SST) gradient (Koutavas & Joanides, 2012); (h) left, the concentration of macrocharcoal in the Toushe Basin as a proxy for local fire (this study), and right, microcharcoal/pollen ratio in the Toushe Basin as a proxy for regional fire (this study).